Robust Classification via a Single Diffusion Model

Huanran Chen [1 2] **Yinpeng Dong** [2 3] **Zhengyi Wang** [2] **Xiao Yang** [2] **Chengqi Duan** [2] **Hang Su** [2 4] **Jun Zhu** [2 3]

Abstract

Diffusion models have been applied to improve adversarial robustness of image classifiers by purifying the adversarial noises or generating realistic data for adversarial training. However, diffusion-based purification can be evaded by stronger adaptive attacks while adversarial training does not perform well under unseen threats, exhibiting inevitable limitations of these methods. To better harness the expressive power of diffusion models, this paper proposes Robust Diffusion Classifier (RDC), a generative classifier that is constructed from a pre-trained diffusion model to be adversarially robust. RDC first maximizes the data likelihood of a given input and then predicts the class probabilities of the optimized input using the conditional likelihood estimated by the diffusion model through Bayes' theorem. To further reduce the computational cost, we propose a new diffusion backbone called multi-head diffusion and develop efficient sampling strategies. As RDC does not require training on particular adversarial attacks, we demonstrate that it is more generalizable to defend against multiple unseen threats. In particular, RDC achieves 75.67% robust accuracy against various ℓ_∞ norm-bounded adaptive attacks with $\epsilon_\infty = 8/255$ on CIFAR-10, surpassing the previous state-of-the-art adversarial training models by $+4.77\%$. The results highlight the potential of generative classifiers by employing pre-trained diffusion models for adversarial robustness compared with the commonly studied discriminative classifiers. Code is available at https://github.com/huanranchen/DiffusionClassifier.

[1]School of Computer Science, Beijing Institute of Technology [2]Dept. of Comp. Sci. and Tech., Institute for AI, Tsinghua-Bosch Joint ML Center, THBI Lab, BNRist Center, Tsinghua University, Beijing, 100084, China [3]RealAI [4]Zhongguancun Laboratory, Beijing, 100080, China. Correspondence to: Jun Zhu <dcszj@tsinghua.edu.cn>.

Proceedings of the 41^{st} International Conference on Machine Learning, Vienna, Austria. PMLR 235, 2024.

1. Introduction

A longstanding problem of deep learning is the vulnerability to adversarial examples (Szegedy et al., 2014; Goodfellow et al., 2015), which are maliciously generated by applying human-imperceptible perturbations to natural examples, but can cause deep learning models to make erroneous predictions. As the adversarial robustness problem leads to security threats in real-world applications (e.g., face recognition (Sharif et al., 2016; Dong et al., 2019), autonomous driving (Cao et al., 2021; Jing et al., 2021), healthcare (Finlayson et al., 2019)), there is a lot of work on defending against adversarial examples, such as adversarial training (Madry et al., 2018; Zhang et al., 2019; Wang et al., 2023b), image denoising (Liao et al., 2018; Samangouei et al., 2018; Song et al., 2018), certified defenses (Raghunathan et al., 2018; Wong & Kolter, 2018; Cohen et al., 2019).

Recently, diffusion models have emerged as a powerful family of generative models, consisting of a forward diffusion process that gradually perturbs data with Gaussian noise and a reverse generative process that learns to remove noise from the perturbed data (Sohl-Dickstein et al., 2015; Ho et al., 2020; Nichol & Dhariwal, 2021; Song et al., 2021). Some researchers have tried to apply diffusion models to improving adversarial robustness in different ways. For example, the adversarial images can be purified through the forward and reverse processes of diffusion models before feeding into the classifier (Blau et al., 2022; Nie et al., 2022; Wang et al., 2022). Besides, the generated data from diffusion models can significantly improve adversarial training (Rebuffi et al., 2021; Wang et al., 2023b), achieving the state-of-the-art results on robustness benchmarks (Croce et al., 2020). These works show promise of diffusion models in the field of adversarial robustness.

However, the existing methods have some limitations. On one hand, the diffusion-based purification approach incurs much more randomness compared to conventional methods, and can be effectively attacked by using the exact gradient and a proper step size [1]. We observe that the adversarial example cannot make the diffusion model output an image

[1]We lower the robust accuracy of DiffPure (Nie et al., 2022) from 71.29% to 44.53% under the ℓ_∞ norm with $\epsilon_\infty = 8/255$, and from 80.60% to 75.59% under the ℓ_2 norm with $\epsilon_2 = 0.5$, as shown in Table 1.

of a different class, but the perturbation is not completely removed. Therefore, the poor robustness of diffusion-based purification is largely due to the vulnerability of downstream classifiers. On the other hand, although adversarial training methods using data generated by diffusion models achieve excellent performance, they are usually not generalizable across different threats (Tramèr & Boneh, 2019; Nie et al., 2022). In summary, these methods leverage diffusion models to improve adversarial robustness of discriminative classifiers, but discriminative learning cannot capture the underlying structure of data distribution, making it hard to control the predictions of inputs outside the training distribution (Schott et al., 2019). As a generative approach, diffusion models provide a more accurate estimation of score function (i.e., the gradient of log-density at the data point) across the entire data space (Song & Ermon, 2019; Song et al., 2021), which also have the potential to provide accurate class probabilities. Therefore, we devote to exploring *how to convert a diffusion model into a generative classifier for improved adversarial robustness?*

In this paper, we propose Robust Diffusion Classifier (**RDC**), a generative classifier obtained from a single pre-trained diffusion model to achieve adversarial robustness. Our method calculates the class probability $p(y|\mathbf{x})$ using the conditional likelihood $p_\theta(\mathbf{x}|y)$ estimated by a diffusion model through Bayes' theorem. The conditional likelihood is approximated by the variational lower bound, which involves calculating the noise prediction loss for every class under different noise levels. In order to reduce time complexity induced by the number of classes, we propose a new UNet backbone named **multi-head diffusion** by modifying the last convolutional layer to output noise predictions of all classes simultaneously. Theoretically, we validate that the optimal diffusion model can achieve absolute robustness under common threat models. However, the practical diffusion model may have an inaccurate density estimation $p_\theta(\mathbf{x}|y)$ or a large gap between the likelihood and its lower bound, leading to inferior performance. To address this issue, we further propose **Likelihood Maximization** as a pre-optimization step to move the input data to regions of high likelihoods before feeding into the diffusion classifier. Our RDC, directly constructed from a pre-trained diffusion model without training on specific adversarial attacks, can perform robust classification under various threat models.

We empirically compare our method with various state-of-the-art methods against strong adaptive attacks, which are integrated with AutoAttack (Croce & Hein, 2020) for more comprehensive evaluations. Specifically, at each step, we obtain the gradient through adaptive attacks (e.g., BPDA, exact gradient) and then feed the gradient into AutoAttack to perform update. Additionally, we investigate the gradient randomness and find that the gradient variance in our method is exceptionally low. This suggests that, due to the low variance and precise gradient, our method does not result in obfuscated gradients (Athalye et al., 2018), indicating that the evaluation is accurate and reliable. On CIFAR-10 (Krizhevsky & Hinton, 2009), RDC achieves 75.67% robust accuracy under the ℓ_∞ norm threat model with $\epsilon_\infty = 8/255$, exhibiting a $+4.77\%$ improvement over the state-of-the-art adversarial training method (Wang et al., 2023b), and a $+3.01\%$ improvement over the state-of-the-art dynamic defenses and randomized defenses (Pérez et al., 2021; Blau et al., 2023). Under unseen threats, RDC leads to a more significant improvement ($> 30\%$) over adversarial training models, DiffPure (Nie et al., 2022) and generative classifiers. Our results disclose the potential of generative models for solving the adversarial robustness problem.

2. Related work

Adversarial robustness. Adversarial examples (Szegedy et al., 2014; Goodfellow et al., 2015) are widely studied in the literature, which are generated by adding imperceptible perturbations to natural examples, but can mislead deep learning models. Many adversarial attack methods (Carlini & Wagner, 2017; Athalye et al., 2018; Dong et al., 2018; Madry et al., 2018; Chen et al., 2023; Croce & Hein, 2020) have been proposed to improve the attack success rate under the white-box or black-box settings, which can be used to evaluate model robustness. To defend against adversarial attacks, adversarial training (Madry et al., 2018; Zhang et al., 2019) stands out as the most effective method, which trains neural networks using adversarially augmented data. However, these models tend to exhibit robustness only to a specific attack they are trained with, and have poor generalization ability to unseen threats (Tramèr & Boneh, 2019; Laidlaw et al., 2021). Another popular approach is adversarial purification (Liao et al., 2018; Samangouei et al., 2018; Song et al., 2018; Nie et al., 2022), which denoises the input images for classification. Most of these defenses cause obfuscated gradients (Athalye et al., 2018) and can be evaded by adaptive attacks (Tramer et al., 2020).

Generative classifiers. Generative classifiers, like naive Bayes (Ng & Jordan, 2001), predict the class probabilities $p(y|\mathbf{x})$ for a given input $\mathbf{x}$ by modeling the data likelihood $p(\mathbf{x}|y)$ using generative models. Compared with discriminative classifiers, generative classifiers are often more robust and well-calibrated (Raina et al., 2003; Schott et al., 2019; Li et al., 2019; Mackowiak et al., 2021; Chen et al., 2024). Modern generative models like diffusion models (Ho et al., 2020; Song et al., 2021) and energy-based models (LeCun et al., 2006; Du & Mordatch, 2019) can also be used as generative classifiers. SBGC (Zimmermann et al., 2021) utilizes a score-based model to calculate the log-likelihood $\log p(\mathbf{x}|y)$ by integration and calculates $p(y|\mathbf{x})$ via Bayes' theorem. HybViT (Yang et al., 2022) learns the joint like-

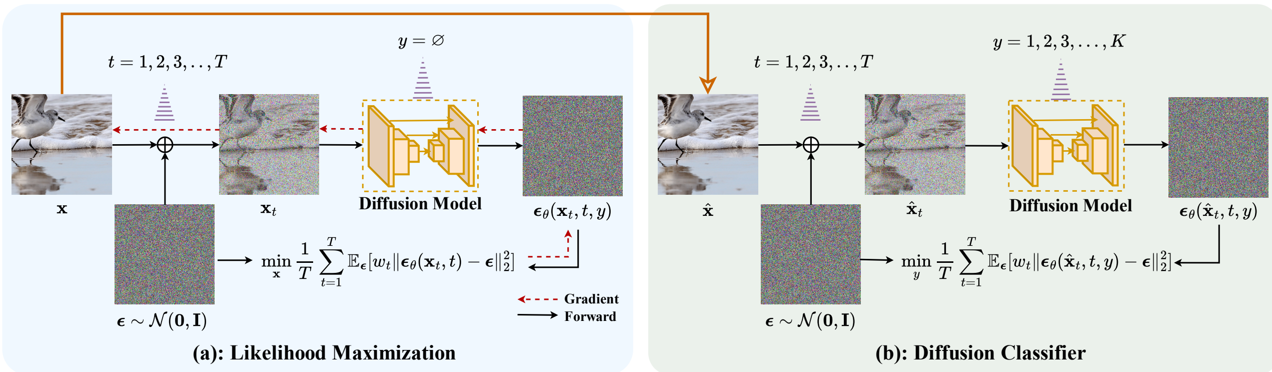

Figure 1. Illustration of our proposed Robust Diffusion Classifier (RDC). Given an input image $\mathbf{x}$, our approach first maximizes the data likelihood (Left) and then classifies the optimized image $\hat{\mathbf{x}}$ with a diffusion model (Right). The class probability $p(y|\hat{\mathbf{x}})$ is given by the conditional log-likelihood $\log p_\theta(\hat{\mathbf{x}}|y)$, which is approximated by the variational lower bound involving calculating the noise prediction error (i.e., diffusion loss) averaged over different timesteps for every class.

lihood $\log p(\mathbf{x}, y) = \log p(\mathbf{x}) + \log p(y|\mathbf{x})$ by training a diffusion model to learn $\log p(\mathbf{x})$ and a standard classifier to model $\log p(y|\mathbf{x})$ at training time, and directly predicts $p(y|\mathbf{x})$ at test time. JEM (Grathwohl et al., 2019) utilizes the energy-based model to predict joint likelihood $\log p(\mathbf{x}, y)$ and applies Bayes' theorem to get $p(y|\mathbf{x})$. We also compare with these generative classifiers in experiments. Recently, diffusion models have also been used for generative classification. Hoogeboom et al. (2021) and Han et al. (2022) perform diffusion process in logit space to learn the categorial classification distribution. Concurrent work (Clark & Jaini, 2023; Li et al., 2023) converts diffusion models to generative classifiers in a similar way to ours, but they focus on zero-shot classification while do not consider adversarial robustness.

Diffusion models for adversarial robustness. As a powerful family of generative models (Dhariwal & Nichol, 2021; Rombach et al., 2022), diffusion models have been introduced to further improve adversarial robustness. DiffPure (Nie et al., 2022) utilizes diffusion models to purify adversarial perturbations by first adding Gaussian noise to input images and then denoising the images. Diffusion models can also help to improve the certified robustness with randomized smoothing (Carlini et al., 2023; Xiao et al., 2023; Zhang et al., 2023; Chen et al., 2024). Besides, using data generated by diffusion models can significantly improve the performance of adversarial training (Rebuffi et al., 2021; Wang et al., 2023b). However, DiffPure is vulnerable to stronger adaptive attacks while adversarial training models do not generalize well across different threat models, as shown in Table 1. A potential reason of their problems is that they still rely on discriminative classifiers, which do not capture the underlying structure of data distribution. As diffusion models have more accurate score estimation in the whole data space, we aim to explore whether a diffusion model itself can be leveraged to build a robust classifier.

3. Methodology

In this section, we present our **Robust Diffusion Classifier (RDC)**, a generative classifier constructed from a pre-trained diffusion model. We first provide an overview of diffusion models in Sec. 3.1, then present how to convert a (class-conditional) diffusion model into a diffusion classifier in Sec. 3.2 with a robustness analysis considering the optimal setting in Sec. 3.3, and finally detail the likelihood maximization and time complexity reduction techniques to further improve the robustness and efficiency in Sec. 3.4 and Sec. 3.5, respectively. Fig. 1 illustrates our approach.

3.1. Preliminary: diffusion models

We briefly review discrete-time diffusion models (Ho et al., 2020). Given $\mathbf{x} := \mathbf{x}_0$ from a real data distribution $q(\mathbf{x}_0)$, the forward diffusion process gradually adds Gaussian noise to the data to obtain a sequence of noisy samples $\{\mathbf{x}_t\}_{t=1}^T$ according to a scaling schedule $\{\alpha_t\}_{t=1}^T$ and a noise schedule $\{\sigma_t\}_{t=1}^T$ as

$$q(\mathbf{x}_t|\mathbf{x}_0) = \mathcal{N}(\mathbf{x}_t; \sqrt{\alpha_t}\mathbf{x}_0, \sigma_t^2\mathbf{I}). \tag{1}$$

Assume that the signal-to-noise ratio $\text{SNR}(t) = \alpha_t/\sigma_t^2$ is strictly monotonically decreasing in time, the sample $\mathbf{x}_t$ is increasingly noisy during the forward process. The scaling and noise schedules are prescribed such that $\mathbf{x}_T$ is nearly an isotropic Gaussian distribution.

The reverse process for Eq. (1) is defined as a Markov chain aimed to approximate $q(\mathbf{x}_0)$ by gradually denoising from the standard Gaussian distribution $p(\mathbf{x}_T) = \mathcal{N}(\mathbf{x}_T; \mathbf{0}, \mathbf{I})$:

$$\begin{aligned} p_\theta(\mathbf{x}_{0:T}) &= p(\mathbf{x}_T)\prod_{t=1}^{T} p_\theta(\mathbf{x}_{t-1}|\mathbf{x}_t), \\ p_\theta(\mathbf{x}_{t-1}|\mathbf{x}_t) &= \mathcal{N}(\mathbf{x}_{t-1}; \boldsymbol{\mu}_\theta(\mathbf{x}_t, t), \tilde{\sigma}_t^2\mathbf{I}), \end{aligned} \tag{2}$$

where $\boldsymbol{\mu}_\theta$ is generally parameterized by a time-conditioned noise prediction network $\boldsymbol{\epsilon}_\theta(\mathbf{x}_t, t)$ (Ho et al., 2020; Kingma et al., 2021):

$$\boldsymbol{\mu}_\theta(\mathbf{x}_t, t) = \sqrt{\frac{\alpha_{t-1}}{\alpha_t}}\left(\mathbf{x}_t - \frac{\sigma_t^2 - \frac{\alpha_t}{\alpha_{t-1}}\sigma_{t-1}^2}{\sigma_t}\boldsymbol{\epsilon}_\theta(\mathbf{x}_t, t)\right). \tag{3}$$

The reverse process can be learned by optimizing the variational lower bound on log-likelihood as

$$\begin{aligned}\log p_\theta(\mathbf{x}) \geq& \mathbb{E}_q[-D_{\mathrm{KL}}(q(\mathbf{x}_T|\mathbf{x}_0)\|p(\mathbf{x}_T)) + \log p_\theta(\mathbf{x}_0|\mathbf{x}_1) \\ &- \sum_{t>1} D_{\mathrm{KL}}(q(\mathbf{x}_{t-1}|\mathbf{x}_t, \mathbf{x}_0)\|p_\theta(\mathbf{x}_{t-1}|\mathbf{x}_t))] \\ =& -\mathbb{E}_{\boldsymbol{\epsilon},t}\left[w_t\|\boldsymbol{\epsilon}_\theta(\mathbf{x}_t, t) - \boldsymbol{\epsilon}\|_2^2\right] + C_1,\end{aligned} \tag{4}$$

where $\mathbb{E}_{\boldsymbol{\epsilon},t}[w_t\|\boldsymbol{\epsilon}_\theta(\mathbf{x}_t, t) - \boldsymbol{\epsilon}\|_2^2]$ is called the *diffusion loss* (Kingma et al., 2021), $\boldsymbol{\epsilon}$ follows the standard Gaussian distribution $\mathcal{N}(\mathbf{0}, \mathbf{I})$, $\mathbf{x}_t = \sqrt{\alpha_t}\mathbf{x}_0 + \sigma_t\boldsymbol{\epsilon}$ given by Eq. (1), C_1 is typically small and can be dropped (Ho et al., 2020; Song et al., 2021), and $w_t = \frac{\sigma_t\alpha_{t-1}}{2\tilde{\sigma}_t^2(1-\alpha_t)\alpha_t}$. To improve the sample quality in practice, Ho et al. (2020) consider a reweighted variant by setting $w_t = 1$.

Similar to Eq. (4), the conditional diffusion model $p_\theta(\mathbf{x}|y)$ can be parameterized by $\boldsymbol{\epsilon}_\theta(\mathbf{x}_t, t, y)$, while the unconditional model $p_\theta(\mathbf{x})$ can be viewed as a special case with a null input as $\boldsymbol{\epsilon}_\theta(\mathbf{x}_t, t) = \boldsymbol{\epsilon}_\theta(\mathbf{x}_t, t, y = \varnothing)$. A similar lower bound on the conditional log-likelihood is

$$\log p_\theta(\mathbf{x}|y) \geq -\mathbb{E}_{\boldsymbol{\epsilon},t}\left[w_t\|\boldsymbol{\epsilon}_\theta(\mathbf{x}_t, t, y) - \boldsymbol{\epsilon}\|_2^2\right] + C, \tag{5}$$

where C is another negligible small constant.

3.2. Diffusion model for classification

Given an input $\mathbf{x}$, a classifier predicts a probability $p_\theta(y|\mathbf{x})$ for class $y \in \{1, 2, .., K\}$ over all K classes and outputs the most probable class as $\tilde{y} = \arg\max_y p_\theta(y|\mathbf{x})$. Popular discriminative approaches train Convolutional Neural Networks (Krizhevsky et al., 2012; He et al., 2016) or Vision Transformers (Dosovitskiy et al., 2020; Liu et al., 2021) to directly learn the conditional probability $p_\theta(y|\mathbf{x})$. However, these discriminative classifiers cannot predict accurately for adversarial example $\mathbf{x}^*$ that is close to the real example $\mathbf{x}$ under the ℓ_p norm as $\|\mathbf{x}^* - \mathbf{x}\|_p \leq \epsilon_p$, since it is hard to control how inputs are classified outside the training distribution (Schott et al., 2019).

On the other hand, diffusion models are trained to provide accurate density estimation over the entire data space (Ho et al., 2020; Song & Ermon, 2019; Song et al., 2021). By transforming a diffusion model into a generative classifier through Bayes' theorem as $p_\theta(y|\mathbf{x}) \propto p_\theta(\mathbf{x}|y)p(y)$, we hypothesize that the classifier can also give a more accurate conditional probability $p_\theta(y|\mathbf{x})$ in the data space, leading to better adversarial robustness. In this paper, we assume a uniform prior $p(y) = 1/K$ for simplicity, which is common for most of the datasets (Krizhevsky & Hinton, 2009; Russakovsky et al., 2015). We show how to compute the conditional probability $p_\theta(y|\mathbf{x})$ via a diffusion model in the following theorem.

Theorem 3.1. *(Proof in Appendix A.1) Let* $d(\mathbf{x}, y, \theta) = \log p_\theta(\mathbf{x}|y) + \mathbb{E}_{\boldsymbol{\epsilon},t}[w_t\|\boldsymbol{\epsilon}_\theta(\mathbf{x}_t, t, y) - \boldsymbol{\epsilon}\|_2^2]$ *denote the gap between the log-likelihood and the diffusion loss. Assume that y is uniformly distributed as $p(y) = \frac{1}{K}$. If $d(\mathbf{x}, y, \theta) \to 0$ for all y, the conditional probability $p_\theta(y|\mathbf{x})$ is*

$$p_\theta(y|\mathbf{x}) = \frac{\exp(-\mathbb{E}_{\boldsymbol{\epsilon},t}[w_t\|\boldsymbol{\epsilon}_\theta(\mathbf{x}_t, t, y) - \boldsymbol{\epsilon}\|_2^2])}{\sum_{\hat{y}} \exp(-\mathbb{E}_{\boldsymbol{\epsilon},t}[w_t\|\boldsymbol{\epsilon}_\theta(\mathbf{x}_t, t, \hat{y}) - \boldsymbol{\epsilon}\|_2^2])}. \tag{6}$$

In Theorem 3.1, we approximate the conditional likelihood with its variational lower bound, which holds true when the gap $d(\mathbf{x}, y, \theta)$ is 0. In practice, although there is inevitably a gap between the log-likelihood and the diffusion loss, we show that the approximation works well in experiments. Eq. (6) requires calculating the noise prediction error over the expectation of random noise $\boldsymbol{\epsilon}$ and timestep t, which is efficiently estimated with the variance reduction technique introduced in Sec. 3.5. Although we assume a uniform prior $p(y) = 1/K$ in Theorem 3.1, our method is also applicable for non-uniform priors by adding $\log p(y)$ to the logit of class y, where $p(y)$ can be estimated from the training data. Below, we provide an analysis on the adversarial robustness of the diffusion classifier in Eq. (6) under the optimal setting.

3.3. Robustness analysis under the optimal setting

To provide a deeper understanding of the robustness of our diffusion classifier, we provide a new theoretical result on the optimal solution of the diffusion model (i.e., diffusion model that has minimal diffusion loss over both the training set and the test set), as shown in the following theorem.

Theorem 3.2. *(Proof in Appendix A.2.1) Let D denote a set of examples and $D_y \subset D$ denote a subset whose ground-truth label is y. The optimal diffusion model $\boldsymbol{\epsilon}_{\theta_D^*}(\mathbf{x}_t, t, y)$ on the set D is the conditional expectation of $\boldsymbol{\epsilon}$:*

$$\boldsymbol{\epsilon}_{\theta_D^*}(\mathbf{x}_t, t, y) = \sum_{\mathbf{x}^{(i)} \in D_y} \frac{1}{\sigma_t} s(\mathbf{x}_t, \mathbf{x}^{(i)}) \cdot (\mathbf{x}_t - \sqrt{\alpha_t}\mathbf{x}^{(i)}) \tag{7}$$

where $s(\mathbf{x}_t, \mathbf{x}^{(i)})$ is the probability that $\mathbf{x}_t$ comes from $\mathbf{x}^{(i)}$:

$$s(\mathbf{x}_t, \mathbf{x}^{(i)}) = \frac{\exp(-\frac{1}{2\sigma_t^2}\|\mathbf{x}_t - \sqrt{\alpha_t}\mathbf{x}^{(i)}\|_2^2)}{\sum_{\mathbf{x}^{(j)} \in D_y} \exp(-\frac{1}{2\sigma_t^2}\|\mathbf{x}_t - \sqrt{\alpha_t}\mathbf{x}^{(j)}\|_2^2)}$$

Given the optimal diffusion model in Eq. (7), we can easily obtain the optimal diffusion classifier by substituting the solution in Eq. (7) into Eq. (6).

Corollary 3.3. *(Proof in Appendix A.2.2) The conditional probability* $p_{\theta_D^*}(y|\mathbf{x})$ *given the optimal diffusion model* $\boldsymbol{\epsilon}_{\theta_D^*}(\mathbf{x}_t, t, y)$ *is* $p_{\theta_D^*}(y|\mathbf{x}) = \mathrm{softmax}\left(f_{\theta_D^*}(\mathbf{x})\right)_y$, *where*

$$f_{\theta_D^*}(\mathbf{x})_y = -\mathbb{E}_{\boldsymbol{\epsilon},t}\left[\frac{\alpha_t}{\sigma_t^2}\Big\|\sum_{\mathbf{x}^{(i)}\in D_y} s(\mathbf{x},\mathbf{x}^{(i)},\boldsymbol{\epsilon},t)\cdot(\mathbf{x}-\mathbf{x}^{(i)})\Big\|_2^2\right],$$

$$s(\mathbf{x},\mathbf{x}^{(i)},\boldsymbol{\epsilon},t) = \frac{\exp\left(-\frac{\|\sqrt{\alpha_t}\mathbf{x}+\sigma_t\boldsymbol{\epsilon}-\sqrt{\alpha_t}\mathbf{x}^{(i)}\|_2^2}{2\sigma_t^2}\right)}{\sum_{\mathbf{x}^{(j)}\in D_y}\exp\left(-\frac{\|\sqrt{\alpha_t}\mathbf{x}+\sigma_t\boldsymbol{\epsilon}-\sqrt{\alpha_t}\mathbf{x}^{(j)}\|_2^2}{2\sigma_t^2}\right)}.$$

Remark. Intuitively, the optimal diffusion classifier utilizes the ℓ_2 norm of the weighted average difference between the input example $\mathbf{x}$ and the real examples $\mathbf{x}^{(i)}$ of class y to calculate the logit for $\mathbf{x}$. The classifier will predict a label $\tilde{y}$ for an input $\mathbf{x}$ if it lies more closely to real examples belonging to $D_{\tilde{y}}$. Moreover, the ℓ_2 norm is averaged with weight $\frac{\alpha_t}{\sigma_t^2}$. As $\frac{\alpha_t}{\sigma_t^2}$ is monotonically decreasing w.r.t. t, the classifier gives small weights for noisy examples and large weights for clean examples, which is reasonable since the noisy examples do not play an important role in classification.

Given this theoretical result, we can readily analyze the problem in diffusion models and diffusion classifiers by comparing the optimal solution with the empirical one. We evaluate the robust accuracy of the optimal diffusion classifier under the ℓ_∞ norm with $\epsilon_\infty = 8/255$ and the ℓ_2 norm with $\epsilon_2 = 0.5$ by AutoAttack (Croce & Hein, 2020). Since our method does not cause obfuscated gradients (as discussed in Sec. 4.4 and Appendix B.2), the robustness evaluation is accurate. We find that the optimal diffusion classifier achieves 100% robust accuracy, validating our hypothesis that the accurate density estimation of diffusion models facilitates robust classification. However, the diffusion models are not optimal in practice. Our trained diffusion classifier can only achieve 35.94% and 76.95% robust accuracy under the ℓ_∞ and ℓ_2 threats, as shown in Table 1.

To figure out the problem, we examine the empirical model and the optimal one on adversarial examples. We find that the diffusion loss $\mathbb{E}_{\boldsymbol{\epsilon},t}[w_t\|\boldsymbol{\epsilon}_\theta(\mathbf{x}_t, t, y) - \boldsymbol{\epsilon}\|_2^2]$ of the empirical model is much larger. It is caused by either the inaccurate density estimation of $p_\theta(\mathbf{x}|y)$ of the diffusion model or the large gap between the log-likelihood and the diffusion loss violating $d(\mathbf{x}, y, \theta) \to 0$. Developing a better conditional diffusion model can help to address this issue, but we leave this to future work. In the following section, we propose an optimization-based algorithm as an alternative strategy to solve both problems simultaneously with a pre-trained diffusion model.

3.4. Likelihood maximization

To address the above problem, a straightforward approach is to minimize the diffusion loss $\mathbb{E}_{\boldsymbol{\epsilon},t}[w_t\|\boldsymbol{\epsilon}_\theta(\mathbf{x}_t, t, y) - \boldsymbol{\epsilon}\|_2^2]$ w.r.t. $\mathbf{x}$ such that the input can escape from the region that the pre-trained diffusion model cannot provide an accurate density estimation or the gap between the likelihood and diffusion loss $d(\mathbf{x}, y, \theta)$ is large. However, we do not know the ground-truth label of $\mathbf{x}$, making the optimization infeasible. As an alternative strategy, we propose to minimize the unconditional diffusion loss as

Algorithm 1 Robust Diffusion Classifier (RDC)

Require: A pre-trained diffusion model $\boldsymbol{\epsilon}_\theta$, input image $\mathbf{x}$, optimization budget η, step size γ, optimization steps N, momentum decay factor μ.

Initialize: $\mathbf{m} = 0, \hat{\mathbf{x}} = \mathbf{x}$;
for $n = 0$ **to** $N-1$ **do**
  Estimate $\mathbf{g} = \nabla_{\mathbf{x}}\mathbb{E}_{\boldsymbol{\epsilon},t}[w_t\|\boldsymbol{\epsilon}_\theta(\hat{\mathbf{x}}_t, t) - \boldsymbol{\epsilon}\|_2^2]$ using one randomly sampled t and $\boldsymbol{\epsilon}$;
  Update momentum $\mathbf{m} = \mu\cdot\mathbf{m} - \frac{\mathbf{g}}{\|\mathbf{g}\|_1}$;
  Update $\hat{\mathbf{x}}$ by $\hat{\mathbf{x}} = \mathrm{clip}_{\mathbf{x},\eta}(\hat{\mathbf{x}} + \gamma\cdot\mathbf{m})$;
end for
Calculate $\mathbb{E}_{\boldsymbol{\epsilon},t}[w_t\|\boldsymbol{\epsilon}_\theta(\hat{\mathbf{x}}_t, t, y) - \boldsymbol{\epsilon}\|_2^2]$ for all $y \in \{1, 2, ..., K\}$ simultaneously using multi-head diffusion;
Calculate $p_\theta(y|\mathbf{x})$ by Eq. (6);
Return: $\tilde{y} = \arg\max_y p_\theta(y|\mathbf{x})$.

$$\min_{\hat{\mathbf{x}}} \mathbb{E}_{\boldsymbol{\epsilon},t}[w_t\|\boldsymbol{\epsilon}_\theta(\hat{\mathbf{x}}_t, t) - \boldsymbol{\epsilon}\|_2^2], \quad \text{s.t. } \|\hat{\mathbf{x}} - \mathbf{x}\|_\infty \leq \eta, \quad (8)$$

which maximizes the lower bound of the log-likelihood in Eq. (4), and thus it can not only minimize the gap $d(\mathbf{x}, \theta)$, but also increase the likelihood $p(\mathbf{x})$. We call this approach **Likelihood Maximization**. In Eq. (8), we restrict the ℓ_∞ norm between the optimized input $\hat{\mathbf{x}}$ and the original input $\mathbf{x}$ to be smaller than η, in order to avoid optimizing $\hat{\mathbf{x}}$ into the region of other classes. We solve the problem in Eq. (8) by gradient-based optimization with N steps.

This method can be also viewed as a new diffusion-based purification defense. On one hand, Xiao et al. (2023) prove that for purification defense, a higher likelihood and a smaller distance to the real data of the purified input $\hat{\mathbf{x}}$ tends to result in better robustness. Compared to DiffPure, our method restricts the optimization budget by η, leading to a smaller distance to the real data. Besides, unlike DiffPure which only maximizes the likelihood with a high probability (Xiao et al., 2023), we directly maximize the likelihood, leading to improved robustness. On the other hand, the adversarial example usually lies in the vicinity of its corresponding real example of the ground-truth class y, thus moving along the direction towards higher $\log p(\mathbf{x})$ will probably lead to higher $\log p(\mathbf{x}|y)$. Therefore, the optimized input $\hat{\mathbf{x}}$ could be more accurately classified by the diffusion classifier.

3.5. Time complexity reduction

Accelerating diffusion classifier. A common practice for estimating the diffusion loss in Eq. (6) is to adopt the Monte Carlo sampling. However, this will lead to a high variance

Table 1. Clean accuracy (%) and robust accuracy (%) of different methods against unseen threats.

Method	Architecture	Clean Acc	Robust Acc			
			ℓ_∞ norm	ℓ_2 norm	StAdv	Avg
AT-DDPM-ℓ_∞	WRN70-16	88.87	63.28	64.65	4.88	44.27
AT-DDPM-ℓ_2	WRN70-16	93.16	49.41	81.05	5.27	45.24
AT-EDM-ℓ_∞	WRN70-16	93.36	70.90	69.73	2.93	47.85
AT-EDM-ℓ_2	WRN70-16	95.90	53.32	**84.77**	5.08	47.72
PAT-self	AlexNet	75.59	47.07	64.06	39.65	50.26
DiffPure ($t^* = 0.125$)	UNet+WRN70-16	87.50	40.62	75.59	12.89	43.03
DiffPure ($t^* = 0.1$)	UNet+WRN70-16	90.97	44.53	72.65	12.89	43.35
SBGC	UNet	95.04	0.00	0.00	0.00	0.00
HybViT	ViT	95.90	0.00	0.00	0.00	0.00
JEM	WRN28-10	92.90	8.20	26.37	0.05	11.54
LM (ours)	UNet+WRN70-16	87.89	71.68	75.00	87.50	**78.06**
DC (ours)	UNet	93.55	35.94	76.95	**93.55**	**68.81**
RDC (LM+DC) (ours)	UNet	89.85	**75.67**	82.03	89.45	**82.38**

with few samples or high time complexity with many samples. To reduce the variance with affordable computational cost, we directly compute the expectation over t instead of sampling t as

$$\mathbb{E}_{\boldsymbol{\epsilon},t}[w_t\|\boldsymbol{\epsilon}_\theta(\mathbf{x}_t,t,y)-\boldsymbol{\epsilon}\|_2^2] = \frac{\sum_{t=1}^{T}\mathbb{E}_{\boldsymbol{\epsilon}}[w_t\|\boldsymbol{\epsilon}_\theta(\mathbf{x}_t,t,y)-\boldsymbol{\epsilon}\|_2^2]}{T}. \tag{9}$$

Eq. (9) requires to calculate the noise prediction error for all timesteps. For $\boldsymbol{\epsilon}$, we still adopt Monte Carlo sampling, but we show that sampling only one $\boldsymbol{\epsilon}$ is sufficient to achieve good performance. We can further reduce the number of timesteps by systematic sampling that selects the timesteps at a uniform interval. Although it does not lead to an obvious drop in clean accuracy, it will significantly affect robust accuracy as shown in Sec. 4.5, because the objective is no longer strongly correlated with log-likelihood after reducing the number of timesteps.

With this technique, the diffusion classifier requires $K \times T$ NFEs (Number of Function Evaluations), which limits its applicability to large datasets. It is because current diffusion models are designed for image generation tasks. They can only provide noise prediction for one class at a time. To obtain the predictions of all classes in a single forward pass, we propose to modify the last convolutional layer in the UNet backbone to predict noises for K classes (i.e., $K \times 3$ dimensions) simultaneously. Thus, it only requires T NFEs for a single image. We name this novel diffusion backbone as **multi-head diffusions**. More details are in Appendix B.1.

Accelerating likelihood maximization. To further reduce the time complexity of likelihood maximization, for each iteration, instead of calculating the diffusion loss using all timesteps like Eq. (9), we only uniformly sample a single timestep to approximate the expectation of the diffusion loss. Surprisingly, this modification not only reduces the time complexity of likelihood maximization from $O(N \times T)$ to $O(N)$, but also greatly improves the robustness. This is because this likelihood maximization induces more randomness, thus it is more effective to smooth the local extrema. We provide more in-depth analysis in Appendix B.2.

Given the above techniques, the overall algorithm of RDC is outlined in Algorithm 1.

4. Experiments

In this section, we first provide the experimental settings in Sec. 4.1. We then show the effectiveness of our method compared with the state-of-the-art methods in Sec. 4.2 and the generalizability across different threat models in Sec. 4.3. We provide thorough analysis to examine gradient obfuscation in Sec. 4.4 and various ablation studies in Sec. 4.5.

4.1. Experimental settings

Datasets and training details. Following Nie et al. (2022), we randomly select 512 images from the CIFAR-10 test set (Krizhevsky & Hinton, 2009) for evaluation due to the high computational cost of AutoAttack. We also conduct experiments on other datasets and other settings in Appendix B.2. We adopt off-the-shelf conditional diffusion model in Karras et al. (2022) and train our multi-head diffusion as detailed in Appendix B for 100 epochs on CIFAR-10 training set.

Hyperparameters. In likelihood maximization, we set the optimization steps $N = 5$, momentum decay factor $\mu = 1$, optimization budget $\eta = 8/255$ (see Sec. 4.5 for an ablation study), step size $\gamma = 0.1$. For each timestep, we only sample one $\boldsymbol{\epsilon}$ to estimate $\mathbb{E}_{\boldsymbol{\epsilon}}[w_t\|\boldsymbol{\epsilon}_\theta(\mathbf{x}_t,t,y)-\boldsymbol{\epsilon}\|_2^2]$.

Robustness evaluation. Following Nie et al. (2022), we evaluate the clean accuracy and robust accuracy using AutoAttack (Croce & Hein, 2020) under both ℓ_∞ norm of $\epsilon_\infty = 8/255$ and ℓ_2 norm of $\epsilon_2 = 0.5$. To demonstrate the generalization ability towards unseen threat models, we also evaluate the robustness against StAdv (Xiao et al., 2018) with 100 steps under the bound of 0.05. Since computing the gradient through likelihood maximization requires calculating the second-order derivative, we use BPDA (Athalye et al., 2018) as the default adaptive attack, approximating the gradient with an identity mapping. We conduct more comprehensive evaluations of gradient obfuscation in Sec. 4.4, where we show that BPDA is as strong as computing the exact gradient. It is important to note that, except for adaptive attacks on DiffPure (Nie et al., 2022), all other attacks solely modify the back-propagation (e.g., BPDA, exact gradient) or the loss function. The iterative updates are all performed by AutoAttack (Croce & Hein, 2020).

One of our follow-up works also provides a thorough theoretical analysis of the certified robustness of our proposed diffusion classifier. For more details, see Chen et al. (2024).

4.2. Comparison with the state-of-the-art

We compare our method with the state-of-the-art defense methods, including adversarial training with DDPM generated data (AT-DDPM) (Rebuffi et al., 2021), with EDM generated data (AT-EDM) (Wang et al., 2023b), and DiffPure (Nie et al., 2022). We also compare with perceptual adversarial training (PAT-self) (Laidlaw et al., 2021) and other generative classifiers, including SBGC (Zimmermann et al., 2021), HybViT (Yang et al., 2022), and JEM (Grathwohl et al., 2019). Notably, robust accuracy of most baselines does not change much on our selected subset. Additionally, we compare the time complexity and robustness of our model with more methods in Table 3 in Appendix B.2.

DiffPure incurs significant memory usage and substantial randomness, posing challenges for robustness evaluation. Their proposed adjoint method (Nie et al., 2022) is insufficient to measure the model robustness. To mitigate this issue, we employ gradient checkpoints to compute the exact gradient and leverage Expectation Over Time (EOT) to reduce the impact of randomness during optimization. Rather than using the 640 times EOT recommended in Fig. 2(a), we adopt PGD-200 (Madry et al., 2018) with 10 times EOT and a large step size $1/255$ to efficiently evaluate DiffPure.

Table 1 shows the results of Likelihood Maximization (LM), Diffusion Classifier (DC) and Robust Diffusion Classifier (RDC) compared with baselines under the ℓ_∞ and ℓ_2 norm threat models. We can see that the robustness of DC outperforms all previous generative classifiers by a large margin. Specifically, DC improves the robust accuracy over JEM by +27.74% under the ℓ_∞ norm and +50.58% under the ℓ_2 norm. RDC can further improve the performance over DC, which achieves 75.67% and 82.03% robust accuracy under the two settings. Notably, RDC outperforms the previous state-of-the-art model AT-EDM (Wang et al., 2023b) by +4.77% under the ℓ_∞ norm.

Table 2. Robust accuracy (%) of RDC under different adaptive attacks. Note that N is the number of optimization steps in Likelihood Maximization (LM), **not** the number of attack iterations. All iterative updates during these attacks are consistently conducted by AutoAttack.

LM steps (N)	Attack	Clean Acc	Robust Acc
5	BPDA	89.85	75.67
5	Lagrange	89.85	77.54
1	Exact Gradient	90.71	69.53
1	BPDA	90.71	69.92

4.3. Defense against unseen threats

Adversarial training methods often suffer from poor generalization across different threat models, while DiffPure requires adjusting purification noise scales for different threat models, which limits their applicability in real-world scenarios where the threat models are unknown. In contrast, our proposed methods are agnostic to specific threat models. To demonstrates the strong generalization ability of our methods across different threat models, we evaluate the generalization performance of our proposed method by testing against different threats, including ℓ_∞, ℓ_2, and StAdv.

Table 1 presents the results, demonstrating that the average robustness of our methods surpasses the baselines by more than 30%. Specifically, RDC outperforms ℓ_∞ adversarial training models by +12.30% under the ℓ_2 norm and ℓ_2 adversarial training models by +22.35% under the ℓ_∞ norm. Impressively, LM, DC and RDC achieve 87.50%, 93.55% and 89.45% robustness under StAdv, surpassing previous methods by more than 53.90%. These results indicate the strong generalization ability of our method and its potential to be applied in real-world scenarios under unknown threats.

4.4. Evaluation of gradient obfuscation

The Diffusion Classifier (DC) can be directly evaluated using AutoAttack. However, the Robust Diffusion Classifier (RDC) cannot be directly assessed with AutoAttack since attacking Likelihood Maximization (LM) requires calculating the second-order derivative of the diffusion loss. In this section, we analyze both gradient randomness and gradient magnitude (in Appendix B.2), demonstrating that ***our method does not result in gradient obfuscation***. Furthermore, we establish that ***our method attains nearly identical robustness under both exact gradient attack and BPDA attack***. These findings compellingly affirm that our method is genuinely robust rather than being overestimated by (potentially) insufficient evaluations.

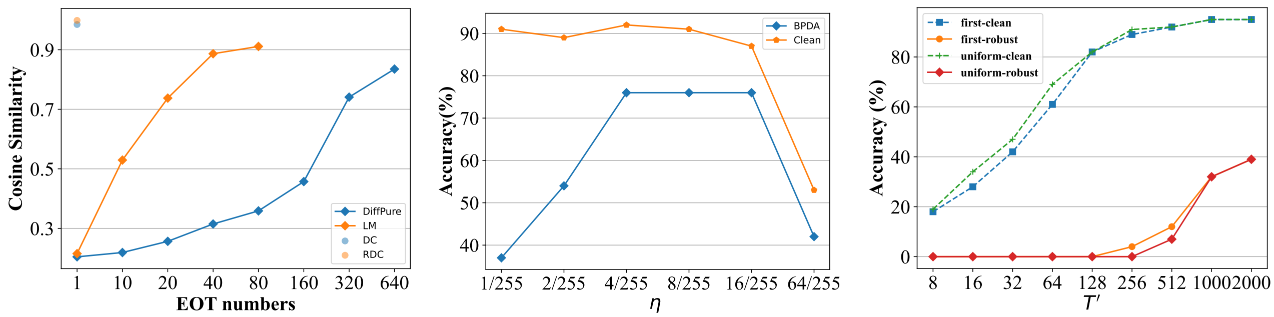

(a) Randomness (b) Ablation of η (c) T'

Figure 2. (a): Randomness of different methods. (b-c): Ablation studies of η and T'.

Exact gradient attack. To directly evaluate the robustness of RDC, we utilize gradient checkpoint and create a computational graph during backpropagation to obtain exact gradients. However, we could only evaluate RDC when the number of optimization steps N in Likelihood Maximization (LM) is $N = 1$ (Note that this is not the number of attack iterations) due to the large memory cost for computing the second-order derivative. As shown in Table 2, our RDC with $N = 1$ achieves 69.53% robust accuracy under the exact gradient attack, about 0.39% lower than BPDA. This result suggests that BPDA suffices for evaluating RDC.

Lagrange attack. RDC optimizes the unconditional diffusion loss before feeding the inputs into DC. If our adversarial examples already have a small unconditional diffusion loss or a large $\log p(\mathbf{x})$, it may not be interrupted during Likelihood Maximization (LM). Therefore, to produce adversarial examples with a small diffusion loss, we set our loss function as

$$\log p_\theta(y|\mathbf{x}) + l \cdot \mathbb{E}_{\boldsymbol{\epsilon},t}[w_t\|\boldsymbol{\epsilon}_\theta(\mathbf{x}_t, t) - \boldsymbol{\epsilon}\|_2^2], \qquad (10)$$

where $p_\theta(y|\mathbf{x})$ is given by Eq. (6), and the first term is the (negative) cross-entropy loss to induce misclassification. For an input, we craft adversarial examples using three different weights, $l = 0, 1, 10$. If one of these three loss functions successfully generates an adversarial example, we count it as a successful attack. As shown in Table 2, this adaptive attack is no more effective than BPDA.

Gradient randomness. To quantify the randomness, we compute the gradients of each model w.r.t. the input ten times and compute the pairwise cosine similarity between the gradients. We then average these cosine similarities across 100 images. To capture the randomness when using EOT, we treat the gradients obtained after applying EOT as a single time and repeat the same process to compute their cosine similarity. As shown in Fig. 2(a), the gradients of our methods exhibit low randomness, while DiffPure is more than 640 times as random as DC, RDC, and about 16 times as random as LM. Thus, the robustness of our methods is not primarily due to the stochasticity of gradients.

4.5. Ablation studies

In this section, we perform ablation studies of several hyperparameters with the first 100 examples in the CIFAR-10 test set. All the experiments are done under AutoAttack with BPDA of ℓ_∞ bounded perturbations with $\epsilon_\infty = 8/255$.

Optimization budget η. To find the best optimization budget η, we test the robust accuracy of different optimization budgets. As shown in Fig. 2(b), the robust accuracy first increases and then decreases as η becomes larger. When η is small, we could not move $\mathbf{x}$ out of the adversarial region. However, when η is too large, we may optimize $\mathbf{x}$ into an image of another class. Therefore, we should choose an appropriate η. In this work, we set $\eta = 8/255$.

Sampling timesteps. We also attempt to reduce the number of timesteps used in calculating the diffusion loss. Since only the DC is influenced by this parameter, we conduct this experiment exclusively on DC to minimize the impact of other factors. One way is to only calculate the diffusion loss of the first T' timesteps $\{i\}_{i=1}^{T'}$ ("first-clean" and "first-robust" in Fig. 2(c)). Inspired by Song et al. (2020), another way is to use systematic sampling, where we use timesteps $\{iT/T'\}_{i=1}^{T'}$ ("uniform-clean" and "uniform-robust" in Fig. 2(c)). Both methods achieve similar results on clean accuracy and robust accuracy. Although a significant reduction of T' does not lead to an obvious drop in clean accuracy, it will significantly affect robust accuracy due to the reason discussed in Sec. 3.5.

Sampling steps for $\boldsymbol{\epsilon}$. We also attempt to improve the estimation of $\mathbb{E}_{\boldsymbol{\epsilon}}[w_t\|\boldsymbol{\epsilon}_\theta(\mathbf{x}_t, t, y) - \boldsymbol{\epsilon}\|_2^2]$ by sampling $\boldsymbol{\epsilon}$ multiple times or keeping $\boldsymbol{\epsilon}$ the same for different timesteps or different classes. However, these increase neither robustness nor accuracy because we have already computed T times for the expectation over t. From another perspective, the cosine similarity of the gradients is about 98.48%, suggesting that additional sampling of $\boldsymbol{\epsilon}$ or using the same $\boldsymbol{\epsilon}$ is unnecessary.

5. Conclusion

In this paper, we propose a novel defense method called Robust Diffusion Classifier (RDC), which leverages a single diffusion model to directly classify input images by predicting data likelihood by diffusion model and calculating class probabilities through Bayes' theorem. We theoretically analyze the robustness of our diffusion classifier, propose to maximize the log-likelihood before feeding the input images into the diffusion classifier. We also propose multi-head diffusion which greatly reduces the time complexity of RDC. We evaluate our method with strong adaptive attacks and conduct extensive experiments. Our method achieves state-of-the-art robustness against these strong adaptive attacks and generalizes well to unseen threat models.

Impact Statement

The emergence of adversarial threats in machine learning, especially in critical areas such as autonomous vehicles, healthcare, and financial systems, calls for more robust defense mechanisms. Our work introduces the Robust Diffusion Classifier, a novel framework that harnesses the capabilities of diffusion models for adversarial robustness in image classification. This approach not only contributes to reinforcing the security of machine learning models against adversarial attacks but also demonstrates significant potential in leveraging diffusion models for adversarial robustness. Our findings set a new precedent in the field and could be inspireful in enhancing trust in AI applications. While our work primarily focuses on adversarial robustness, it opens avenues for further research for diffusion models in reliability and resilience, moving towards a future where machine learning can reliably function even in adversarially challenging environments.

Acknowledgements

This work was supported by the National Natural Science Foundation of China (Nos. 62276149, 92370124, 62350080, 92248303, U2341228, 62061136001, 62076147), BNRist (BNR2022RC01006), Tsinghua Institute for Guo Qiang, and the High Performance Computing Center, Tsinghua University. Y. Dong was also supported by the China National Postdoctoral Program for Innovative Talents. J. Zhu was also supported by the XPlorer Prize.

References

Athalye, A., Carlini, N., and Wagner, D. Obfuscated gradients give a false sense of security: Circumventing defenses to adversarial examples. In *International Conference on Machine Learning*, pp. 274–283, 2018.

Blau, T., Ganz, R., Kawar, B., Bronstein, A., and Elad, M. Threat model-agnostic adversarial defense using diffusion models. *arXiv preprint arXiv:2207.08089*, 2022.

Blau, T., Ganz, R., Baskin, C., Elad, M., and Bronstein, A. Classifier robustness enhancement via test-time transformation. *arXiv preprint arXiv:2303.15409*, 2023.

Cao, Y., Wang, N., Xiao, C., Yang, D., Fang, J., Yang, R., Chen, Q. A., Liu, M., and Li, B. Invisible for both camera and lidar: Security of multi-sensor fusion based perception in autonomous driving under physical-world attacks. In *2021 IEEE Symposium on Security and Privacy*, pp. 176–194, 2021.

Carlini, N. and Wagner, D. Towards evaluating the robustness of neural networks. In *IEEE Symposium on Security and Privacy*, pp. 39–57, 2017.

Carlini, N., Tramer, F., Dvijotham, K. D., Rice, L., Sun, M., and Kolter, J. Z. (certified!!) adversarial robustness for free! In *International Conference on Learning Representations*, 2023.

Chen, H., Zhang, Y., Dong, Y., Yang, X., Su, H., and Zhu, J. Rethinking model ensemble in transfer-based adversarial attacks. In *The Twelfth International Conference on Learning Representations*, 2023.

Chen, H., Dong, Y., Shao, S., Hao, Z., Yang, X., Su, H., and Zhu, J. Your diffusion model is secretly a certifiably robust classifier. *arXiv preprint arXiv:2402.02316*, 2024.

Clark, K. and Jaini, P. Text-to-image diffusion models are zero-shot classifiers. *arXiv preprint arXiv:2303.15233*, 2023.

Cohen, J., Rosenfeld, E., and Kolter, Z. Certified adversarial robustness via randomized smoothing. In *International Conference on Machine Learning*, pp. 1310–1320, 2019.

Croce, F. and Hein, M. Reliable evaluation of adversarial robustness with an ensemble of diverse parameter-free attacks. In *International Conference on Machine Learning*, pp. 2206–2216, 2020.

Croce, F., Andriushchenko, M., Sehwag, V., Debenedetti, E., Flammarion, N., Chiang, M., Mittal, P., and Hein, M. Robustbench: a standardized adversarial robustness benchmark. In *Thirty-fifth Conference on Neural Information Processing Systems Datasets and Benchmarks Track*, 2020.

Debenedetti, E., Sehwag, V., and Mittal, P. A light recipe to train robust vision transformers. *arXiv preprint arXiv:2209.07399*, 2022.

Dhariwal, P. and Nichol, A. Diffusion models beat gans on image synthesis. *Advances in Neural Information Processing Systems*, pp. 8780–8794, 2021.

Dong, M., Chen, X., Wang, Y., and Xu, C. Random normalization aggregation for adversarial defense. *Advances in Neural Information Processing Systems*, pp. 33676–33688, 2022.

Dong, Y., Liao, F., Pang, T., Su, H., Zhu, J., Hu, X., and Li, J. Boosting adversarial attacks with momentum. In *Proceedings of the IEEE/CVF Conference on Computer Vision and Pattern Recognition*, pp. 9185–9193, 2018.

Dong, Y., Su, H., Wu, B., Li, Z., Liu, W., Zhang, T., and Zhu, J. Efficient decision-based black-box adversarial attacks on face recognition. In *Proceedings of the IEEE/CVF Conference on Computer Vision and Pattern Recognition*, pp. 7714–7722, 2019.

Dong, Y., Chen, H., Chen, J., Fang, Z., Yang, X., Zhang, Y., Tian, Y., Su, H., and Zhu, J. How robust is google's bard to adversarial image attacks? *arXiv preprint arXiv:2309.11751*, 2023.

Dosovitskiy, A., Beyer, L., Kolesnikov, A., Weissenborn, D., Zhai, X., Unterthiner, T., Dehghani, M., Minderer, M., Heigold, G., Gelly, S., et al. An image is worth 16x16 words: Transformers for image recognition at scale. In *International Conference on Learning Representations*, 2020.

Du, Y. and Mordatch, I. Implicit generation and modeling with energy based models. *Advances in Neural Information Processing Systems*, 2019.

Engstrom, L., Ilyas, A., Salman, H., Santurkar, S., and Tsipras, D. Robustness (python library), 2019. URL https://github.com/MadryLab/robustness.

Finlayson, S. G., Bowers, J. D., Ito, J., Zittrain, J. L., Beam, A. L., and Kohane, I. S. Adversarial attacks on medical machine learning. *Science*, pp. 1287–1289, 2019.

Fu, Y., Yu, Q., Li, M., Chandra, V., and Lin, Y. Double-win quant: Aggressively winning robustness of quantized deep neural networks via random precision training and inference. In *International Conference on Machine Learning*, pp. 3492–3504, 2021.

Goodfellow, I. J., Shlens, J., and Szegedy, C. Explaining and harnessing adversarial examples. In *International Conference on Learning Representations*, 2015.

Grathwohl, W., Wang, K.-C., Jacobsen, J.-H., Duvenaud, D., Norouzi, M., and Swersky, K. Your classifier is secretly an energy based model and you should treat it like one. In *International Conference on Learning Representations*, 2019.

Han, X., Zheng, H., and Zhou, M. Card: Classification and regression diffusion models. *Advances in Neural Information Processing Systems*, pp. 18100–18115, 2022.

Hao, Z., Ying, C., Dong, Y., Su, H., Song, J., and Zhu, J. Gsmooth: Certified robustness against semantic transformations via generalized randomized smoothing. In *International Conference on Machine Learning*, pp. 8465–8483, 2022.

He, K., Zhang, X., Ren, S., and Sun, J. Deep residual learning for image recognition. In *Proceedings of the IEEE/CVF Conference on Computer Vision and Pattern Recognition*, pp. 770–778, 2016.

Ho, J., Jain, A., and Abbeel, P. Denoising diffusion probabilistic models. *Advances in Neural Information Processing Systems*, pp. 6840–6851, 2020.

Hoogeboom, E., Nielsen, D., Jaini, P., Forré, P., and Welling, M. Argmax flows and multinomial diffusion: Learning categorical distributions. *Advances in Neural Information Processing Systems*, pp. 12454–12465, 2021.

Jing, P., Tang, Q., Du, Y., Xue, L., Luo, X., Wang, T., Nie, S., and Wu, S. Too good to be safe: Tricking lane detection in autonomous driving with crafted perturbations. In *Proceedings of USENIX Security Symposium*, pp. 3237–3254, 2021.

Karras, T., Aittala, M., Aila, T., and Laine, S. Elucidating the design space of diffusion-based generative models. *Advances in Neural Information Processing Systems*, pp. 26565–26577, 2022.

Kingma, D., Salimans, T., Poole, B., and Ho, J. Variational diffusion models. *Advances in Neural Information Processing Systems*, pp. 21696–21707, 2021.

Krizhevsky, A. and Hinton, G. Learning multiple layers of features from tiny images. Technical report, University of Toronto, 2009.

Krizhevsky, A., Sutskever, I., and Hinton, G. E. Imagenet classification with deep convolutional neural networks. In *Advances in Neural Information Processing Systems*, 2012.

Laidlaw, C., Singla, S., and Feizi, S. Perceptual adversarial robustness: Defense against unseen threat models. In *International Conference on Learning Representations*, 2021.

LeCun, Y., Chopra, S., Hadsell, R., Ranzato, M., and Huang, F. A tutorial on energy-based learning. *Predicting structured data*, 1(0), 2006.

Li, A. C., Prabhudesai, M., Duggal, S., Brown, E., and Pathak, D. Your diffusion model is secretly a zero-shot classifier. *arXiv preprint arXiv:2303.16203*, 2023.

Li, Y., Bradshaw, J., and Sharma, Y. Are generative classifiers more robust to adversarial attacks? In *International Conference on Machine Learning*, pp. 3804–3814, 2019.

Liao, F., Liang, M., Dong, Y., Pang, T., Hu, X., and Zhu, J. Defense against adversarial attacks using high-level representation guided denoiser. In *Proceedings of the IEEE/CVF Conference on Computer Vision and Pattern Recognition*, pp. 1778–1787, 2018.

Liu, X., Zhang, X., Ma, J., Peng, J., and Liu, Q. Instaflow: One step is enough for high-quality diffusion-based text-to-image generation. *arXiv preprint arXiv:2309.06380*, 2023.

Liu, Z., Lin, Y., Cao, Y., Hu, H., Wei, Y., Zhang, Z., Lin, S., and Guo, B. Swin transformer: Hierarchical vision transformer using shifted windows. In *Proceedings of the IEEE/CVF International Conference on Computer Vision*, pp. 10012–10022, 2021.

Mackowiak, R., Ardizzone, L., Kothe, U., and Rother, C. Generative classifiers as a basis for trustworthy image classification. In *Proceedings of the IEEE/CVF Conference on Computer Vision and Pattern Recognition*, pp. 2971–2981, 2021.

Madry, A., Makelov, A., Schmidt, L., Tsipras, D., and Vladu, A. Towards deep learning models resistant to adversarial attacks. In *International Conference on Learning Representations*, 2018.

Ng, A. Y. and Jordan, M. I. On discriminative vs. generative classifiers: a comparison of logistic regression and naive bayes. In *Proceedings of the 14th International Conference on Neural Information Processing Systems: Natural and Synthetic*, pp. 841–848, 2001.

Nichol, A. Q. and Dhariwal, P. Improved denoising diffusion probabilistic models. In *International Conference on Machine Learning*, pp. 8162–8171, 2021.

Nie, W., Guo, B., Huang, Y., Xiao, C., Vahdat, A., and Anandkumar, A. Diffusion models for adversarial purification. In *International Conference on Machine Learning*, pp. 16805–16827, 2022.

Papamakarios, G., Pavlakou, T., and Murray, I. Masked autoregressive flow for density estimation. *Advances in neural information processing systems*, 30, 2017.

Pérez, J. C., Alfarra, M., Jeanneret, G., Rueda, L., Thabet, A., Ghanem, B., and Arbeláez, P. Enhancing adversarial robustness via test-time transformation ensembling. In *Proceedings of the IEEE/CVF International Conference on Computer Vision*, pp. 81–91, 2021.

Poole, B., Jain, A., Barron, J. T., and Mildenhall, B. Dreamfusion: Text-to-3d using 2d diffusion. In *The Eleventh International Conference on Learning Representations*, 2022.

Raghunathan, A., Steinhardt, J., and Liang, P. Certified defenses against adversarial examples. In *International Conference on Learning Representations*, 2018.

Raina, R., Shen, Y., Ng, A. Y., and McCallum, A. Classification with hybrid generative/discriminative models. In *Proceedings of the 16th International Conference on Neural Information Processing Systems*, pp. 545–552, 2003.

Rebuffi, S.-A., Gowal, S., Calian, D. A., Stimberg, F., Wiles, O., and Mann, T. Fixing data augmentation to improve adversarial robustness. *arXiv preprint arXiv:2103.01946*, 2021.

Rombach, R., Blattmann, A., Lorenz, D., Esser, P., and Ommer, B. High-resolution image synthesis with latent diffusion models. In *Proceedings of the IEEE/CVF Conference on Computer Vision and Pattern Recognition*, pp. 10684–10695, 2022.

Russakovsky, O., Deng, J., Su, H., Krause, J., Satheesh, S., Ma, S., Huang, Z., Karpathy, A., Khosla, A., Bernstein, M., et al. Imagenet large scale visual recognition challenge. *International journal of computer vision*, 115(3): 211–252, 2015.

Sabour, S., Cao, Y., Faghri, F., and Fleet, D. J. Adversarial manipulation of deep representations. *arXiv preprint arXiv:1511.05122*, 2015.

Salman, H., Ilyas, A., Engstrom, L., Kapoor, A., and Madry, A. Do adversarially robust imagenet models transfer better? *Advances in Neural Information Processing Systems*, 33:3533–3545, 2020.

Samangouei, P., Kabkab, M., and Chellappa, R. Defense-gan: Protecting classifiers against adversarial attacks using generative models. In *International Conference on Learning Representations*, 2018.

Schott, L., Rauber, J., Bethge, M., and Brendel, W. Towards the first adversarially robust neural network model on mnist. In *International Conference on Learning Representations*, 2019.

Schwinn, L., Bungert, L., Nguyen, A., Raab, R., Pulsmeyer, F., Precup, D., Eskofier, B., and Zanca, D. Improving robustness against real-world and worst-case distribution shifts through decision region quantification. In *International Conference on Machine Learning*, pp. 19434–19449, 2022.

Shao, S., Dai, X., Yin, S., Li, L., Chen, H., and Hu, Y. Catch-up distillation: You only need to train once for accelerating sampling. *arXiv preprint arXiv:2305.10769*, 2023.

Sharif, M., Bhagavatula, S., Bauer, L., and Reiter, M. K. Accessorize to a crime: Real and stealthy attacks on state-of-the-art face recognition. In *ACM Sigsac Conference on Computer and Communications Security*, pp. 1528–1540, 2016.

Sohl-Dickstein, J., Weiss, E., Maheswaranathan, N., and Ganguli, S. Deep unsupervised learning using nonequilibrium thermodynamics. In *International Conference on Machine Learning*, pp. 2256–2265, 2015.

Song, J., Meng, C., and Ermon, S. Denoising diffusion implicit models. In *International Conference on Learning Representations*, 2020.

Song, Y. and Ermon, S. Generative modeling by estimating gradients of the data distribution. In *Proceedings of the 33rd International Conference on Neural Information Processing Systems*, pp. 11918–11930, 2019.

Song, Y., Kim, T., Nowozin, S., Ermon, S., and Kushman, N. Pixeldefend: Leveraging generative models to understand and defend against adversarial examples. In *International Conference on Learning Representations*, 2018.

Song, Y., Sohl-Dickstein, J., Kingma, D. P., Kumar, A., Ermon, S., and Poole, B. Score-based generative modeling through stochastic differential equations. In *International Conference on Learning Representations*, 2021.

Song, Y., Dhariwal, P., Chen, M., and Sutskever, I. Consistency models. *arXiv preprint arXiv:2303.01469*, 2023.

Szegedy, C., Zaremba, W., Sutskever, I., Bruna, J., Erhan, D., Goodfellow, I., and Fergus, R. Intriguing properties of neural networks. *International Conference on Learning Representations*, 2014.

Tramèr, F. and Boneh, D. Adversarial training and robustness for multiple perturbations. In *Proceedings of the 33rd International Conference on Neural Information Processing Systems*, pp. 5866–5876, 2019.

Tramer, F., Carlini, N., Brendel, W., and Madry, A. On adaptive attacks to adversarial example defenses. In *Advances in Neural Information Processing Systems*, pp. 1633–1645, 2020.

Tsipras, D., Santurkar, S., Engstrom, L., Turner, A., and Madry, A. Robustness may be at odds with accuracy. In *International Conference on Learning Representations*, 2019.

Wang, J., Lyu, Z., Lin, D., Dai, B., and Fu, H. Guided diffusion model for adversarial purification. *arXiv preprint arXiv:2205.14969*, 2022.

Wang, Z., Lu, C., Wang, Y., Bao, F., Li, C., Su, H., and Zhu, J. Prolificdreamer: High-fidelity and diverse text-to-3d generation with variational score distillation. *arXiv preprint arXiv:2305.16213*, 2023a.

Wang, Z., Pang, T., Du, C., Lin, M., Liu, W., and Yan, S. Better diffusion models further improve adversarial training. *arXiv preprint arXiv:2302.04638*, 2023b.

Wei, Z., Wang, Y., Guo, Y., and Wang, Y. Cfa: Class-wise calibrated fair adversarial training. In *Proceedings of the IEEE/CVF Conference on Computer Vision and Pattern Recognition*, pp. 8193–8201, 2023a.

Wei, Z., Wang, Y., and Wang, Y. Jailbreak and guard aligned language models with only few in-context demonstrations. *arXiv preprint arXiv:2310.06387*, 2023b.

Wierstra, D., Schaul, T., Glasmachers, T., Sun, Y., Peters, J., and Schmidhuber, J. Natural evolution strategies. *The Journal of Machine Learning Research*, pp. 949–980, 2014.

Wong, E. and Kolter, Z. Provable defenses against adversarial examples via the convex outer adversarial polytope. In *International Conference on Machine Learning*, pp. 5286–5295, 2018.

Wong, E., Rice, L., and Kolter, J. Z. Fast is better than free: Revisiting adversarial training. *arXiv preprint arXiv:2001.03994*, 2020.

Xiao, C., Zhu, J.-Y., Li, B., He, W., Liu, M., and Song, D. Spatially transformed adversarial examples. In *International Conference on Learning Representations*, 2018.

Xiao, C., Chen, Z., Jin, K., Wang, J., Nie, W., Liu, M., Anandkumar, A., Li, B., and Song, D. Densepure: Understanding diffusion models for adversarial robustness. In *International Conference on Learning Representations*, 2023.

Yang, X., Shih, S.-M., Fu, Y., Zhao, X., and Ji, S. Your vit is secretly a hybrid discriminative-generative diffusion model. *arXiv preprint arXiv:2208.07791*, 2022.

Zhang, H., Yu, Y., Jiao, J., Xing, E., El Ghaoui, L., and Jordan, M. Theoretically principled trade-off between robustness and accuracy. In *International Conference on Machine Learning*, pp. 7472–7482, 2019.

Zhang, J., Chen, Z., Zhang, H., Xiao, C., and Li, B. {DiffSmooth}: Certifiably robust learning via diffusion models and local smoothing. In *32nd USENIX Security Symposium*, pp. 4787–4804, 2023.

Zhang, Y., He, H., Zhu, J., Chen, H., Wang, Y., and Wei, Z. On the duality between sharpness-aware minimization and adversarial training. In *International Conference on Machine Learning*, 2024.

Zimmermann, R. S., Schott, L., Song, Y., Dunn, B. A., and Klindt, D. A. Score-based generative classifiers. In *NeurIPS 2021 Workshop on Deep Generative Models and Downstream Applications*, 2021.

A. Proofs and Derivations

A.1. Proof of Theorem 3.1

Proof.

$$
\begin{aligned}
p_\theta(y|\mathbf{x}) &= \frac{p_\theta(\mathbf{x}, y)}{\sum_{\hat{y}} p_\theta(\mathbf{x}, \hat{y})} \\
&= \frac{p_\theta(\mathbf{x}|y)p_\theta(y)}{\sum_{y} p_\theta(\mathbf{x}|\hat{y})p_\theta(\hat{y})} \\
&= \frac{p_\theta(\mathbf{x}|y)}{\sum_{\hat{y}} p_\theta(\mathbf{x}|\hat{y})} \\
&= \frac{e^{\log p_\theta(\mathbf{x}|y)}}{\sum_{\hat{y}} e^{\log p_\theta(\mathbf{x}|\hat{y})}} \\
&= \frac{\exp\Big(\mathbb{E}_{\boldsymbol{\epsilon},t}[w_t\|\boldsymbol{\epsilon}_\theta(\mathbf{x}_t, t, y) - \boldsymbol{\epsilon}\|_2^2] + \log p_\theta(\mathbf{x}|y) - \mathbb{E}_{\boldsymbol{\epsilon},t}[w_t\|\boldsymbol{\epsilon}_\theta(\mathbf{x}_t, t, y) - \boldsymbol{\epsilon}\|_2^2]\Big)}{\sum_{\hat{y}} \exp\Big(\mathbb{E}_{\boldsymbol{\epsilon},t}[w_t\|\boldsymbol{\epsilon}_\theta(\mathbf{x}_t, t, \hat{y}) - \boldsymbol{\epsilon}\|_2^2] + \log p_\theta(\mathbf{x}|\hat{y}) - \mathbb{E}_{\boldsymbol{\epsilon},t}[w_t\|\boldsymbol{\epsilon}_\theta(\mathbf{x}_t, t, \hat{y}) - \boldsymbol{\epsilon}\|_2^2]\Big)} \\
&= \frac{\exp\Big(d(\mathbf{x}, y, \theta)\Big)\exp\Big(-\mathbb{E}_{\boldsymbol{\epsilon},t}[w\|\boldsymbol{\epsilon}_\theta(\mathbf{x}_t, t, y) - \boldsymbol{\epsilon}\|_2^2]\Big)}{\sum_{\hat{y}} \exp\Big(d(\mathbf{x}, \hat{y}, \theta)\Big)\exp\Big(-\mathbb{E}_{\boldsymbol{\epsilon},t}[w_t\|\boldsymbol{\epsilon}_\theta(\mathbf{x}_t, t, \hat{y}) - \boldsymbol{\epsilon}\|_2^2]\Big)}.
\end{aligned}
$$

When $\forall \hat{y},\ d(\mathbf{x}, \hat{y}, \theta) \to 0$, we can get:

$$
\forall \hat{y},\ \exp\Big(\mathbb{E}_{\boldsymbol{\epsilon},t}[w_t\|\boldsymbol{\epsilon}_\theta(\mathbf{x}_t, t, \hat{y}) - \boldsymbol{\epsilon}\|_2^2] + \log p_\theta(\mathbf{x}|\hat{y})\Big) \to 1.
$$

Therefore,

$$
p_\theta(y|\mathbf{x}) = \frac{\exp\Big(-\mathbb{E}_{\boldsymbol{\epsilon},t}[w_t\|\boldsymbol{\epsilon}_\theta(\mathbf{x}_t, t, y) - \boldsymbol{\epsilon}\|_2^2]\Big)}{\sum_{\hat{y}} \exp\Big(-\mathbb{E}_{\boldsymbol{\epsilon},t}[w_t\|\boldsymbol{\epsilon}_\theta(\mathbf{x}_t, t, \hat{y}) - \boldsymbol{\epsilon}\|_2^2]\Big)}.
$$

□

A.2. Derivation of the optimal diffusion classifier

A.2.1. Optimal diffusion model: proof of Theorem 3.2

Proof. The optimal diffusion model has the minimal error $\mathbb{E}_{\mathbf{x},t,y}[\|\boldsymbol{\epsilon}(\mathbf{x}_t, t, y) - \boldsymbol{\epsilon}\|_2^2]$ among all the models in hypothesis space. Since the prediction for one input pair $(\mathbf{x}_t, t, y)$ does not affect the prediction for any other input pairs, the optimal diffusion model will give the optimal solution for any input pair $(\mathbf{x}_t, t, y)$:

$$
\mathbb{E}_{\mathbf{x}^{(i)} \sim p(\mathbf{x}^{(i)}|\mathbf{x}_t, y)}[\|\boldsymbol{\epsilon}_{\theta_D^*}(\mathbf{x}_t, t, y) - \boldsymbol{\epsilon}_i\|_2^2] = \min_\theta \mathbb{E}_{\mathbf{x}^{(i)} \sim p(\mathbf{x}^{(i)}|\mathbf{x}_t, y)}[\|\boldsymbol{\epsilon}_\theta(\mathbf{x}_t, t, y) - \boldsymbol{\epsilon}_i\|_2^2],
$$

where $\boldsymbol{\epsilon}_i = \frac{\mathbf{x}_t - \sqrt{\alpha_t}\mathbf{x}^{(i)}}{\sigma_t}$.

Note that

$$
p(\mathbf{x}^{(i)}|\mathbf{x}_t, y) = \frac{p(\mathbf{x}^{(i)}|y)p(\mathbf{x}_t|\mathbf{x}^{(i)}, y)}{p(\mathbf{x}_t|y)} = \frac{p(\mathbf{x}^{(i)}|y)q(\mathbf{x}_t|\mathbf{x}^{(i)})}{p(\mathbf{x}_t|y)}.
$$

Assume that

$$
p(\mathbf{x}^{(i)}|y) = \begin{cases} \frac{1}{|D_y|} & , \mathbf{x}^{(i)} \in D_y \\ 0 & , \mathbf{x}^{(i)} \notin D_y \end{cases}
$$

Solving $\frac{\partial}{\partial \boldsymbol{\epsilon}_\theta(\mathbf{x}_t, t, y)} \mathbb{E}_{\mathbf{x}^{(i)} \sim p(\mathbf{x}^{(i)}|\mathbf{x}_t, y)}[\|\boldsymbol{\epsilon}_\theta(\mathbf{x}_t, t, y) - \boldsymbol{\epsilon}_i\|_2^2] = 0$, we can get:

$$\mathbb{E}_{\mathbf{x}^{(i)}\sim p(\mathbf{x}^{(i)}|\mathbf{x}_t,y)}[\boldsymbol{\epsilon}_\theta(\mathbf{x}_t,t,y)-\boldsymbol{\epsilon}_i]=0,$$
$$\sum_{x^{(i)}\in D} p(\mathbf{x}^{(i)}|\mathbf{x}_t,y)\boldsymbol{\epsilon}_\theta(\mathbf{x}_t,t,y)=\sum_{\mathbf{x}^{(i)}\in D_y} p(\mathbf{x}^{(i)}|\mathbf{x}_t,y)\boldsymbol{\epsilon}_i.$$

Substitute $\boldsymbol{\epsilon}_i$ by Eq. (1):

$$\begin{aligned}
\boldsymbol{\epsilon}_\theta(\mathbf{x}_t,t,y) &= \sum_{\mathbf{x}^{(i)}\in D_y} p(\mathbf{x}^{(i)}|\mathbf{x}_t,y)\frac{\mathbf{x}_t-\sqrt{\alpha_t}\mathbf{x}^{(i)}}{\sigma_t}\\
&= \sum_{\mathbf{x}^{(i)}\in D_y} \frac{p(\mathbf{x}^{(i)}|y)q(\mathbf{x}_t|\mathbf{x}^{(i)})}{p(\mathbf{x}_t|y)}\frac{\mathbf{x}_t-\sqrt{\alpha_t}\mathbf{x}^{(i)}}{\sigma_t}\\
&= \sum_{\mathbf{x}^{(i)}\in D_y} \frac{p(\mathbf{x}^{(i)}|y)}{p(\mathbf{x}_t|y)}p(\mathcal{N}(\mathbf{x}_t|\sqrt{\alpha_t}\mathbf{x}^{(i)},\sigma_t^2 I)=\frac{\mathbf{x}_t-\sqrt{\alpha_t}\mathbf{x}^{(i)}}{\sigma_t})\frac{\mathbf{x}_t-\sqrt{\alpha_t}\mathbf{x}^{(i)}}{\sigma_t}\\
&= \sum_{\mathbf{x}^{(i)}\in D_y} \frac{p(\mathbf{x}^{(i)}|y)}{p(\mathbf{x}_t|y)}\frac{1}{(2\pi\sigma_t)^{\frac{n}{2}}}\exp(-\frac{\|\mathbf{x}_t-\sqrt{\alpha_t}\mathbf{x}^{(i)}\|_2^2}{2\sigma_t^2})\frac{\mathbf{x}_t-\sqrt{\alpha_t}\mathbf{x}^{(i)}}{\sigma_t}
\end{aligned}$$

To avoid numerical problem caused by $\frac{1}{(2\pi\sigma_t)^{\frac{n}{2}}}$ and intractable $\frac{p(\mathbf{x}^{(i)}|y)}{p(\mathbf{x}_t|y)}$, we re-organize this equation using softmax function:

$$\begin{aligned}
\boldsymbol{\epsilon}_\theta(\mathbf{x}_t,t,y) &= \sum_{\mathbf{x}^{(i)}\in D_y} \frac{\frac{p(\mathbf{x}^{(i)}|y)}{p(\mathbf{x}_t|y)}\frac{1}{(2\pi\sigma_t)^{\frac{n}{2}}}\exp(-\frac{\|\mathbf{x}_t-\sqrt{\alpha_t}\mathbf{x}^{(i)}\|_2^2}{2\sigma_t^2})}{\sum_{j=1}^{|D_y|}p(\mathbf{x}_j|\mathbf{x}_t,y)}\frac{\mathbf{x}_t-\sqrt{\alpha_t}\mathbf{x}^{(i)}}{\sigma_t}\\
&= \sum_{\mathbf{x}^{(i)}\in D_y} \frac{\frac{p(\mathbf{x}^{(i)}|y)}{p(\mathbf{x}_t|y)}\frac{1}{(2\pi\sigma_t)^{\frac{n}{2}}}\exp(-\frac{\|\mathbf{x}_t-\sqrt{\alpha_t}\mathbf{x}^{(i)}\|_2^2}{2\sigma_t^2})}{\sum_{j=1}^{|D_y|}\frac{p(\mathbf{x}_j|y)}{p(\mathbf{x}_t|y)}\frac{1}{(2\pi\sigma_t)^{\frac{n}{2}}}\exp(-\frac{\|\mathbf{x}_t-\sqrt{\alpha_t}\mathbf{x}_j\|_2^2}{2\sigma_t^2})}\frac{\mathbf{x}_t-\sqrt{\alpha_t}\mathbf{x}^{(i)}}{\sigma_t}\\
&= \sum_{\mathbf{x}^{(i)}\in D_y} \frac{1}{\sigma_t}(\mathbf{x}_t-\sqrt{\alpha_t}\mathbf{x}^{(i)})\frac{\exp(-\frac{1}{2\sigma_t^2}\|\mathbf{x}_t-\sqrt{\alpha_t}\mathbf{x}^{(i)}\|_2^2)}{\sum_{\mathbf{x}^{(j)}\in D_y}\exp(-\frac{1}{2\sigma_t^2}\|\mathbf{x}_t-\sqrt{\alpha_t}\mathbf{x}^{(j)}\|_2^2)}.
\end{aligned}$$

This is the result of Eq. (7). □

A.2.2. Optimal diffusion classifier: proof of Theorem 3.3

Proof. Substitute Eq. (7) into Eq. (6):

$$\begin{aligned}
&f_{\theta_D^*}(\mathbf{x})_y\\
=&-\mathbb{E}_{t,\boldsymbol{\epsilon}}[\|\boldsymbol{\epsilon}_\theta(\mathbf{x}_t,t,y)-\boldsymbol{\epsilon}\|_2^2]\\
=&-\mathbb{E}_{t,\boldsymbol{\epsilon}}[\|\sum_{\mathbf{x}^{(i)}\in D_y}[\frac{(\mathbf{x}_t-\sqrt{\alpha_t}\mathbf{x}^{(i)})}{\sigma_t}\frac{\exp(-\frac{\|\mathbf{x}_t-\sqrt{\alpha_t}\mathbf{x}^{(i)}\|_2^2}{2\sigma_t^2})}{\sum_{\mathbf{x}^{(j)}\in D_y}\exp(-\frac{\|\mathbf{x}_t-\sqrt{\alpha_t}\mathbf{x}^{(j)}\|_2^2}{2\sigma_t^2})}]-\boldsymbol{\epsilon}\|_2^2]\\
=&-\mathbb{E}_{t,\boldsymbol{\epsilon}}[\|\sum_{\mathbf{x}^{(i)}\in D_y}[\frac{(\sqrt{\alpha_t}\mathbf{x}+\sigma_t\boldsymbol{\epsilon}-\sqrt{\alpha_t}\mathbf{x}^{(i)})}{\sigma_t}\frac{\exp\left(-\frac{\|\sqrt{\alpha_t}\mathbf{x}+\sigma_t\boldsymbol{\epsilon}-\sqrt{\alpha_t}\mathbf{x}^{(i)}\|_2^2}{2\sigma_t^2}\right)}{\sum_{\mathbf{x}^{(j)}\in D_y}\exp\left(-\frac{\|\sqrt{\alpha_t}\mathbf{x}+\sigma_t\boldsymbol{\epsilon}-\sqrt{\alpha_t}\mathbf{x}^{(j)}\|_2^2}{2\sigma_t^2}\right)}]-\boldsymbol{\epsilon}\|_2^2]\\
=&-\mathbb{E}_{t,\boldsymbol{\epsilon}}[\|\sum_{\mathbf{x}^{(i)}\in D_y}[\frac{1}{\sigma_t}(\sqrt{\alpha_t}\mathbf{x}-\sqrt{\alpha_t}\mathbf{x}^{(i)})s(\mathbf{x},\mathbf{x}^{(i)},\boldsymbol{\epsilon},t)+\boldsymbol{\epsilon}\sum_{\mathbf{x}^{(i)}\in D_y}s(\mathbf{x},\mathbf{x}^{(i)},\boldsymbol{\epsilon},t)]\\
=&-\mathbb{E}_{t,\boldsymbol{\epsilon}}[\|\sum_{\mathbf{x}^{(i)}\in D_y}[\frac{1}{\sigma_t}(\sqrt{\alpha_t}\mathbf{x}-\sqrt{\alpha_t}\mathbf{x}^{(i)})s(\mathbf{x},\mathbf{x}^{(i)},\boldsymbol{\epsilon},t)]\|_2^2]\\
=&-\mathbb{E}_{\boldsymbol{\epsilon},t}[\frac{\alpha_t}{\sigma_t^2}\|\sum_{\mathbf{x}^{(i)}\in D_y}s(\mathbf{x},\mathbf{x}^{(i)},\boldsymbol{\epsilon},t)(\mathbf{x}-\mathbf{x}^{(i)})\|_2^2].
\end{aligned}$$

We get the result. □

A.3. Derivation of conditional elbos in Eq. (5)

We provide a derivation of conditional ELBO in the following, which is similar to the unconditional ELBO in Ho et al. (2020).

$$
\begin{aligned}
&\log p_\theta(\mathbf{x}_0|y) \\
=&\log \int \frac{p_\theta(\mathbf{x}_{0:T}|y)q(\mathbf{x}_{1:T}|\mathbf{x}_0,y)}{q(\mathbf{x}_{1:T}|\mathbf{x}_0,y)}d\mathbf{x}_{1:T} \\
=&\log \mathbb{E}_{q(\mathbf{x}_{1:T}|\mathbf{x}_0,y)}[\frac{p_\theta(\mathbf{x}_T|y)p_\theta(\mathbf{x}_{0:T-1}|\mathbf{x}_T,y)}{q(\mathbf{x}_{1:T}|\mathbf{x}_0,y)}] \\
\geq&\mathbb{E}_{q(\mathbf{x}_{1:T}|\mathbf{x}_0,y)}[\log \frac{p_\theta(\mathbf{x}_T|y)p_\theta(\mathbf{x}_{0:T-1}|\mathbf{x}_T,y)}{q(\mathbf{x}_{1:T}|\mathbf{x}_0,y)}] \\
=&\mathbb{E}_{q(\mathbf{x}_{1:T}|\mathbf{x}_0,y)}[\log \frac{p_\theta(\mathbf{x}_T|y)\prod_{i=0}^{T-1}p_\theta(\mathbf{x}_i|\mathbf{x}_{i+1},y)}{\prod_{i=0}^{T-1}q(\mathbf{x}_{i+1}|\mathbf{x}_i,\mathbf{x}_0,y)}] \\
=&\mathbb{E}_{q(\mathbf{x}_{1:T}|\mathbf{x}_0,y)}[\log \frac{p_\theta(\mathbf{x}_T|y)\prod_{i=0}^{T-1}p_\theta(\mathbf{x}_i|\mathbf{x}_{i+1},y)}{\prod_{i=0}^{T-1}\frac{q(\mathbf{x}_{i+1}|\mathbf{x}_0,y)q(\mathbf{x}_i|\mathbf{x}_{i+1},\mathbf{x}_0,y)}{q(\mathbf{x}_i|\mathbf{x}_0,y)}}] \\
=&\mathbb{E}_{q(\mathbf{x}_{1:T}|\mathbf{x}_0,y)}[\log \frac{p_\theta(\mathbf{x}_T|y)\prod_{i=0}^{T-1}p_\theta(\mathbf{x}_i|\mathbf{x}_{i+1},y)}{\prod_{i=0}^{T-1}q(\mathbf{x}_i|\mathbf{x}_{i+1},\mathbf{x}_0,y)} - \log q(\mathbf{x}_T|\mathbf{x}_0,y)] \\
=&\mathbb{E}_{q(\mathbf{x}_{1:T}|\mathbf{x}_0,y)}[\log \frac{\prod_{i=0}^{T-1}p_\theta(\mathbf{x}_i|\mathbf{x}_{i+1},y)}{\prod_{i=0}^{T-1}q(\mathbf{x}_i|\mathbf{x}_{i+1},\mathbf{x}_0,y)} - \log\frac{q(\mathbf{x}_T|\mathbf{x}_0,y)}{p_\theta(\mathbf{x}_T|y)}] \\
=&\sum_{i=0}^{T-1}\mathbb{E}_{q(\mathbf{x}_i,\mathbf{x}_{i+1}|\mathbf{x}_0,y)}[\log \frac{p_\theta(\mathbf{x}_i|\mathbf{x}_{i+1},y)}{q(\mathbf{x}_i|\mathbf{x}_{i+1},\mathbf{x}_0,y)}] - D_{KL}(q(\mathbf{x}_T|\mathbf{x}_0,y)\|p_\theta(\mathbf{x}_T|y)) \\
=&\sum_{i=0}^{T-1}\mathbb{E}_{q(\mathbf{x}_{i+1}|\mathbf{x}_0,y)}\mathbb{E}_{q(\mathbf{x}_i|\mathbf{x}_{i+1},\mathbf{x}_0,y)}[\log \frac{p_\theta(\mathbf{x}_i|\mathbf{x}_{i+1},y)}{q(\mathbf{x}_i|\mathbf{x}_{i+1},\mathbf{x}_0,y)}] - D_{KL}(q(\mathbf{x}_T|\mathbf{x}_0,y)\|p_\theta(\mathbf{x}_T|y)) \\
=&C_4 - \sum_{i=1}^{T-1}\mathbb{E}_{q(\mathbf{x}_{i+1}|\mathbf{x}_0,y)}[D_{KL}(q(\mathbf{x}_i|\mathbf{x}_{i+1},\mathbf{x}_0,y)\|p_\theta(\mathbf{x}_i|\mathbf{x}_{i+1},y))] \\
=&-\mathbb{E}_{\boldsymbol{\epsilon},t}\left[w_t\|\boldsymbol{\epsilon}_\theta(\mathbf{x}_t,t,y)-\boldsymbol{\epsilon}\|_2^2\right]+C.
\end{aligned}
$$

We get the result of Eq. (5).

A.4. Connection between Energy-Based Models (EBMs)

The EBMs (LeCun et al., 2006) directly use neural networks to learn $p_\theta(\mathbf{x})$ and $p_\theta(\mathbf{x}|y)$.

$$
p_\theta(\mathbf{x}|y) = \frac{\exp(-E_\theta(\mathbf{x})_y)}{Z(\theta,y)},
$$

Where $E_\theta(\mathbf{x}) : R^D \to R^n$, and $Z(\theta,y) = \int \exp(-E_\theta(\mathbf{x})_y)d\mathbf{x}$ is the normalizing constant.

As described in Grathwohl et al. (2019), we can use EBMs to classify images by calculating the conditional probability:

$$
p_\theta(y|\mathbf{x}) = \frac{\exp(-E_\theta(\mathbf{x})_y)}{\sum_{\hat{y}}\exp(-E_\theta(\mathbf{x})_{\hat{y}})}. \tag{11}
$$

Compare Eq. (11) and Eq. (6), we can also set the energy function as:

$$
E_\theta(\mathbf{x})_y \approx \mathbb{E}_{t,\boldsymbol{\epsilon}}\left[w_t\|\boldsymbol{\epsilon}_\theta(\mathbf{x}_t,t,y)-\boldsymbol{\epsilon}\|_2^2\right]. \tag{12}
$$

Therefore, our diffusion classifier could be viewed as an EBM, and the energy function is the conditional diffusion loss.

A.5. Computing gradient without computing UNet jacobi

We propose another way to compute the gradient of Eq. (9) without backpropagating through the UNet. Note that we do not use this method in any of the experiments. We only derive this method and conduct some theoretical analysis.

Lemma A.1. *Assuming that* $\mathbf{z} \sim \mathcal{N}(\boldsymbol{\mu}, \boldsymbol{\Sigma}),\ f : \mathbb{R}^{n_i} \to \mathbb{R}^{n_o} \in \mathcal{C}^1,\ \ p : \mathbb{R}^{n_i} \to \mathbb{R} \in \mathcal{C}^1$. *We can get*

$$\nabla_{\boldsymbol{\mu}} \mathbb{E}_{\mathbf{z}}[f(\mathbf{z})] = \mathbb{E}_{\mathbf{z}}[\nabla_{\boldsymbol{\mu}} \log p(\mathbf{z}) f(\mathbf{z})^T]. \tag{13}$$

Proof. Inspired by Wierstra et al. (2014), we derive

$$\begin{aligned}
\nabla_{\boldsymbol{\mu}} E[f(\mathbf{z})] &= \nabla_{\boldsymbol{\mu}} \int f(\mathbf{z}) p(\mathbf{z}|\boldsymbol{\mu}) d\mathbf{z} \\
&= \lim_{d\boldsymbol{\mu} \to \mathbf{0}} \frac{\int f(\mathbf{z}) p(\mathbf{z}|\boldsymbol{\mu} + d\boldsymbol{\mu}) d\mathbf{z} - \int f(\mathbf{z}) p(\mathbf{z}|\boldsymbol{\mu}) d\mathbf{z}}{d\boldsymbol{\mu}} \\
&= \int \nabla_{\boldsymbol{\mu}} p(\mathbf{z}|\boldsymbol{\mu}) f(\mathbf{z})^T d\mathbf{z} \\
&= \int p(\mathbf{z}|\boldsymbol{\mu}) \nabla_{\boldsymbol{\mu}} \log p(\mathbf{z}|\boldsymbol{\mu}) f(\mathbf{z})^T d\mathbf{z} \\
&= \mathbb{E}_z[\nabla_{\boldsymbol{\mu}} \log p(\mathbf{z}|\boldsymbol{\mu}) f(\mathbf{z})^T].
\end{aligned}$$

□

According to Lemma A.1, we can derive the gradient of Eq. (9) as

$$\begin{aligned}
&\frac{d}{d\mathbf{x}} \mathbb{E}_{\boldsymbol{\epsilon}}[\|\boldsymbol{\epsilon}_\theta(\mathbf{x}_t, t) - \boldsymbol{\epsilon}\|_2^2] \\
=&\frac{d}{d\mathbf{x}} \mathbb{E}_{\mathbf{x}_t}[\|\boldsymbol{\epsilon}_\theta(\mathbf{x}_t, t) - \frac{\mathbf{x}_t - \sqrt{\alpha_t}\mathbf{x}}{\sigma_t}\|_2^2] \\
=&\frac{d}{d\mathbf{x}} \mathbb{E}_{\mathbf{x}_t}[g(\mathbf{x}_t, \mathbf{x}, t)] \\
=&\frac{\partial}{\partial \mathbf{x}_t} \mathbb{E}_{\mathbf{x}_t}[g(\mathbf{x}_t, \mathbf{x}, t)] \frac{\partial \mathbf{x}_t}{\partial \mathbf{x}} + \frac{\partial}{\partial \mathbf{x}} \mathbb{E}_{\mathbf{x}_t}[g(\mathbf{x}_t, \mathbf{x}, t)] \\
=&\mathbb{E}_{\mathbf{x}_t}[\frac{\partial \log p(\mathbf{x}_t|\mathbf{x})}{\partial \mathbf{x}} g(\mathbf{x}_t, \mathbf{x}, t)] + \frac{\partial}{\partial \mathbf{x}} \mathbb{E}_{\mathbf{x}_t}[g(\mathbf{x}_t, \mathbf{x}, t)] \\
=&\mathbb{E}_{\mathbf{x}_t}[\frac{\partial \log p(\mathbf{x}_t|\mathbf{x})}{\partial \mathbf{x}} \|\boldsymbol{\epsilon}_\theta(\mathbf{x}_t, t) - \frac{\mathbf{x}_t - \sqrt{\alpha_t}\mathbf{x}}{\sigma_t}\|_2^2] + \mathbb{E}_{\mathbf{x}_t}[2(\boldsymbol{\epsilon}_\theta(\mathbf{x}_t, t) - \frac{\mathbf{x}_t - \sqrt{\alpha_t}\mathbf{x}}{\sigma_t}) \frac{\sqrt{\alpha_t}}{\sigma_t}] \\
=&\mathbb{E}_{\boldsymbol{\epsilon}}[\frac{\partial \log p(\mathbf{x}_t|\mathbf{x})}{\partial \mathbf{x}} \|\boldsymbol{\epsilon}_\theta(\mathbf{x}_t, t) - \boldsymbol{\epsilon}\|_2^2] + \mathbb{E}_{\boldsymbol{\epsilon}}[(\boldsymbol{\epsilon}_\theta(\mathbf{x}_t, t) - \boldsymbol{\epsilon}) \frac{2\sqrt{\alpha_t}}{\sigma_t}].
\end{aligned} \tag{14}$$

Similarly, we can get the gradient of conditional diffusion loss

$$\begin{aligned}
&\frac{d}{d\mathbf{x}} \mathbb{E}_{\boldsymbol{\epsilon}}[\|\boldsymbol{\epsilon}_\theta(\mathbf{x}_t, t, y) - \boldsymbol{\epsilon}\|_2^2] \\
=&\mathbb{E}_{\mathbf{x}_t}[\frac{\partial \log p(\mathbf{x}_t|\mathbf{x})}{\partial \mathbf{x}} \|\boldsymbol{\epsilon}_\theta(\mathbf{x}_t, t, y) - \frac{\mathbf{x}_t - \sqrt{\alpha_t}\mathbf{x}}{\sigma_t}\|_2^2] + \mathbb{E}_{\mathbf{x}_t}[(\boldsymbol{\epsilon}_\theta(\mathbf{x}_t, t, y) - \frac{\mathbf{x}_t - \sqrt{\alpha_t}\mathbf{x}}{\sigma_t}) \frac{2\sqrt{\alpha_t}}{\sigma_t}] \\
=&\mathbb{E}_{\boldsymbol{\epsilon}}[\frac{\partial \log p(\mathbf{x}_t|\mathbf{x})}{\partial \mathbf{x}} \|\boldsymbol{\epsilon}_\theta(\mathbf{x}_t, t, y) - \boldsymbol{\epsilon}\|_2^2] + \mathbb{E}_{\boldsymbol{\epsilon}}[(\boldsymbol{\epsilon}_\theta(\mathbf{x}_t, t, y) - \boldsymbol{\epsilon}) \frac{2\sqrt{\alpha_t}}{\sigma_t}].
\end{aligned} \tag{15}$$

As shown, the gradient of Eq. (9) have two terms. The first term equals to the weighted sum of $\frac{\partial \log p(\mathbf{x}_t|\mathbf{x})}{\partial \mathbf{x}}$. In VE-SDE case, where $\mathbf{x}_t = \mathbf{x} + \sigma_t \boldsymbol{\epsilon}$, the negative gradient direction is aligned with $\mathbf{x} - \mathbf{x}_t$ (a vector starting from $\mathbf{x}_t$ and ending at $\mathbf{x}$). The second term is proportional to the gradient of Score Distillation Sampling (Poole et al., 2022; Wang et al., 2023a), which also point toward real data. Consequently, optimizing the diffusion loss will move $\mathbf{x}$ toward a region with higher log likelihood.

Algorithm 2 Training of multi-head diffusion

Require: A pre-trained diffusion model $\boldsymbol{\epsilon}_\theta$, dataset $\mathcal{D}$, a multi-head diffusion model $\boldsymbol{\epsilon}_\phi$

```
repeat
    x_0, y ~ D;
    t ~ Uniform({1, 2, ..., T}), ε ~ N(0, I);
    for y = 0 to K − 1 do
        Take gradient descent step on ∇_φ E_{ε,t}[w_t ||ε_θ(x̂_t, t, y) − ε_φ(x̂_t, t, y)||_2^2];
    end for
until converged;
```

B. More experimental results

B.1. Training details

Computational resources. We conduct Direct Attack on 1× A40 GPUs due to the large memory cost of computational graphs for second-order derivatives. We use 2× 3090 GPUs for other experiments. We also analyze the time complexity and test the real-time cost on a single 3090 GPU, as demonstrated in Table 3. We are unable to assess the real-time cost of some methods due to difficulties in replicating them.

Training details of multi-head diffusion. To reduce the time complexity of the diffusion classifier from $O(K \times T)$ to $O(T)$, we propose to slightly modify the architecture of the UNet, enabling it to predict for all classes at once. Since our changes are limited to the UNet architecture, all theorems and analyses remain applicable in this context.

However, this architecture only achieves 60% accuracy on the CIFAR10 dataset, even with nearly the same number of parameters as the original UNet. We tried to solve this problem by using a larger CFG (*i.e.*, viewing extrapolated result $(1 + \text{cfg}) \cdot \boldsymbol{\epsilon}_\theta(\mathbf{x}_t, t, y) - \text{cfg} \cdot \boldsymbol{\epsilon}_\theta(\mathbf{x}_t, t)$ as the prediction of UNet), but it does not work.

We hypothesize that with the traditional conditional architecture, the UNet focuses on extracting features relevant to specific class labels, leading to a more accurate prediction of the conditional score. In contrast, multi-head diffusion must extract features suitable for predicting all classes, as different heads use the same features for their predictions. To test this hypothesis, we measure the cosine similarity between features of a given $\mathbf{x}_t$ with different embeddings y. We find that for the traditional diffusion architecture, these features differ from each other. However, for multi-head diffusion, the cosine similarity of these predictions exceeds 0.98, indicating that the predictions are almost identical due to the identical feature.

It's worth noting that this does not mean traditional diffusion models are superior to multi-head diffusion. Both architectures have nearly the same number of parameters, as we only modify the last convolution layer. Additionally, the training loss curve and validation loss curve for both are almost identical, indicating they fit the training distribution and generalize to the data distribution similarly. The FID values of these two models are 3.14 and 3.13, very close to each other. The decreased performance of multi-head diffusion in the diffusion classifier is likely because it isn't clear on which feature to extract first. The training dynamic lets multi-head diffusion extracts features suitable for all classes, leading to similar predictions for each class, similar diffusion loss, and thus lower classification performance.

To prevent predictions for all classes from being too similar, we first considered training the multi-head diffusion with negative examples. Initially, we attempted to train the multi-head diffusion using the cross-entropy loss. While this achieved a training accuracy of 91.79%, the test accuracy only reached 82.48%. Moreover, as training continued, overfitting to the training set became more pronounced. **Notably, this model had 0% robustness.** Fortunately, this experiment underscores the strength of our adaptive attacks in evaluating such randomized defenses, affirming that the robustness of the diffusion classifier is not merely due to its stochastic nature leading to an inadequate evaluation. A lingering concern is our lack of understanding as to why switching the training loss from diffusion loss to cross-entropy loss drastically diminishes the generalization ability and robustness.

Our hypothesis posits that, when trained with the diffusion loss, diffusion models are compelled to extract robust features because they are required to denoise the noisy images. However, when trained using the cross-entropy loss, there isn't a necessity to denoise the noisy images, so the models might not extract robust features. As a result, they may lose their image generation and denoising capabilities, as well as their generalization ability and robustness. We evaluated the diffusion loss of the diffusion models trained by cross-entropy loss and found that their diffusion losses hovered around 10. Furthermore, the images they generated resembled noise, meaning that they lose their generation ability.

Table 3. Clean accuracy (%) and robust accuracy (%) of different methods against unseen threats.

Method	Architecture	NFEs	Real Time (s)	Clean Acc	Robust Acc		
					ℓ_∞ norm	ℓ_2 norm	Avg
AT-DDPM-ℓ_∞	WRN70-16	1	0.01	88.87	63.28	64.65	63.97
AT-DDPM-ℓ_2	WRN70-16	1	0.01	93.16	49.41	81.05	65.23
AT-EDM-ℓ_∞	WRN70-16	1	0.01	93.36	70.90	69.73	70.32
AT-EDM-ℓ_2	WRN70-16	1	0.01	95.90	53.32	84.77	69.05
PAT-self	AlexNet	1	0.01	75.59	47.07	64.06	55.57
DiffPure ($t^* = 0.125$)	UNet	126	0.72	87.50	40.62	75.59	58.11
DiffPure ($t^* = 0.1$)	UNet	101	0.60	90.97	44.53	72.65	58.59
SBGC	UNet	$30TK$	15.78	95.04	0.00	0.00	0.00
HybViT	ViT	1	0.01	95.90	0.00	0.00	0.00
JEM	WRN28-10	1	0.01	92.90	8.20	26.37	17.29
Pérez et al. (2021)	WRN70-16	9	n/a	89.48	72.66	71.09	71.87
Schwinn et al. (2022)	WRN70-16	KN	n/a	90.77	71.00	72.87	71.94
Blau et al. (2023)	WRN70-16	KN	n/a	88.18	72.02	75.90	73.96
LM (ours)	WRN70-16	$1 + NT$	2.50	95.04	2.34	12.5	7.42
LM (ours)	WRN70-16	$1 + N$	0.10	87.89	71.68	75.00	**73.34**
DC (ours)	UNet	TK	9.76	93.55	35.94	76.95	**55.45**
RDC (ours)	UNet	$NT + TK$	12.26	93.16	73.24	80.27	**76.76**
RDC (ours)	UNet	$N + TK$	9.86	88.18	**80.07**	**84.76**	**82.42**
RDC (ours)	UNet	$N + T$	1.43	89.85	75.67	82.03	**78.85**

To address this issue, we need to strike a balance between the diffusion loss, which ensures the robustness of the diffusion models, and the negative example loss (e.g., cross-entropy loss, CW loss, DLR loss) to prevent their predictions for various classes from becoming too similar. This balancing act turns the training of multi-head diffusion into a largely hyper-parameter tuning endeavor. To circumvent such a complex training process, we suggest distilling the multi-head diffusion from a pretrained traditional diffusion model. As illustrated in Algorithm 2, the primary distinction between multi-head diffusion distillation and traditional diffusion model training is that the predictions for all classes provided by the multi-head diffusion model are simultaneously aligned with those of a pre-trained diffusion model.

Note that in Algorithm 2, the predictions for different classes are computed in parallel. This approach sidesteps the need for tedious hyper-parameter tuning. Nevertheless, there's still potential for refinement. In this algorithm, the input pair $(\mathbf{x}_t, t, y)$ is not sampled based on its probability $p(\mathbf{x}_t, t, y) = \int p(\mathbf{x}|y)p(t)p(\mathbf{x}_t|\mathbf{x})p(y)d\mathbf{x}$. This could be why the multi-head diffusion slightly underperforms compared to the traditional diffusion model. Addressing this issue might involve using importance sampling, a potential avenue for future research.

B.2. More Analysis and Discussion

Gradient magnitude. When attacking the diffusion classifiers, we need to take the derivative of the diffusion loss. This process is similar to what is done when training diffusion models, so gradient vanishing is unlikely to occur. We also measure the average absolute value of the gradient (*i.e.*, $\frac{1}{D}\|g\|_1$). As shown in Table 4, the magnitude of the gradient in our method is on the same scale as that of other adversarial training models, validating that our method does not suffer from gradient vanishing.

Table 4. Gradient magnitudes.

Method	$\frac{1}{D}\|g\|_1$
Engstrom et al. (2019)	7.7×10^{-6}
Wong et al. (2020)	1.1×10^{-5}
Salman et al. (2020)	6.6×10^{-6}
Debenedetti et al. (2022)	9.8×10^{-6}
Ours	8.2×10^{-6}

Substituting likelihood maximization with DiffPure. We further study the performance by substituting likelihood maximization with DiffPure. We use the same hyperparameters as in Nie et al. (2022) and follow the identical evaluation setup as described in Sec. 4.1. The robustness of each method under the ℓ_∞-norm threat model with $\epsilon_\infty = 8/255$ on the CIFAR-10 dataset is shown in Table 5. As shown, DC+DiffPure outperforms DiffPure significantly, highlighting the effectiveness of our diffusion classifier. Furthermore, RDC surpasses DC+DiffPure, indicating that likelihood maximization is more compatible with the diffusion classifier. Besides, Xiao et al. (2023) provide an interesting explanation of DiffPure. It has been demonstrated that DiffPure increases the likelihood of inputs with high probability, resulting in better robustness. By directly maximizing the likelihood of inputs, our likelihood maximization further enhances the potential for improved robustness.

Attacking using the adaptive attack in Sabour et al. (2015). Tramer et al. (2020) propose to add an additional feature loss (Sabour et al., 2015) that minimizes the class score between the current image and a target image in another class. This create adversarial examples whose class scores match those of clean examples but belong to a different class, thereby generating in-manifold adversarial examples, avoiding to be detected by likelihood-based adversarial example detectors. To evaluate the robustness of our method against these adaptive attacks, we integrate them with AutoAttack and test the robust accuracy under ℓ_∞ threat model with $\epsilon_\infty = 8/255$. Surprisingly, our method achieves 90.04% robustness against attack using feature loss, and 86.72% robustness against attack using feature loss combined with the cross entropy loss or DLR loss in AutoAttack. On one hand, our Lagrange attack in Sec. 4.4 directly maximizes the lower bound of likelihood, making it more effective than feature loss. On the other hand, our method does not incorporate adversarial example detectors, making it unnecessary to strictly align the logits of adversarial examples with those of clean images.

Table 5. The robustness of DiffPure, DiffPure+DC and RDC.

Method	Robustness(%)
DiffPure	53.52
DiffPure+DC	69.92
RDC	75.67

Comparison with other dynamic defenses. We also compare our methods with state-of-the-art dynamic defenses. As some of these methods have not yet been open-sourced, we reference the best results reported in their respective papers. We use N to denote the optimization steps in their methods (*e.g.*, qualification steps in Schwinn et al. (2022), PGD steps in Blau et al. (2023)). As shown in Table 3, our methods are not only more efficient but also effective than these dynamic defenses. Specifically, the time complexities of these dynamic defenses are related to the number of classes K, which limits their applicability in large datasets. On the contrary, the time complexity of our RDC does not depend on K. Moreover, our RDC outperforms previous methods by +3.01% on ℓ_∞ robustness and +6.33% on ℓ_2 robustness, demonstrating the strong efficacy and efficiency of our RDC.

Comparison with other randomized defenses. As shown in Table 6, our method outperforms previous state-of-the-art randomized defenses. This is because diffusion models are naturally robust to such Gaussian corruptions, and such high variance Gaussian corruptions are much more effective than Fu et al. (2021); Dong et al. (2022) to smooth the local extrema in loss landscape, preventing the existence of adversarial examples. Our method can also be integrated with randomized smoothing to get certified robustness. For more detail, refer to Chen et al. (2024).

Table 6. Comparison with other randomized defenses.

Method	Attacker	Robustness(%)
Fu et al. (2021)	PGD-100	66.28
Dong et al. (2022)	PGD-20	60.69
Hao et al. (2022)	n/a	0
RDC (Ours)	AutoAttack	75.67

Comparison between different likelihood maximizations. We compare the LM $(1 + NT)$ with the improved version LM $(1 + N)$. Surprisingly, under the BPDA attack, LM $(1 + NT)$ achieves only 2.34% robustness. On the one hand, the likelihood maximization moves the inputs towards high log-likelihood region estimated by diffusion models, instead of traditional classifiers, thus it is more effective when combined with diffusion classifiers. On the other hand, although the diffusion losses of LM $(1 + NT)$ and LM $(1 + N)$ are same in expectation, the former induces less randomness, thus it is less effective to smooth the local extrema. LLet's delve into a special case with $N = 1$. In this case, the expectation of LM $(1 + NT)$ is $\mathbb{E}_{\boldsymbol{\epsilon}}[f(\mathbf{x} + \nabla_{\mathbf{x}}\mathbb{E}_t[w_t\|\boldsymbol{\epsilon}_\theta(\mathbf{x}_t, t, y) - \boldsymbol{\epsilon}\|_2^2])]$, while the expectation of LM $(1 + N)$ is $\mathbb{E}_{\boldsymbol{\epsilon},t}[f(\mathbf{x} + \nabla_{\mathbf{x}}[w_t\|\boldsymbol{\epsilon}_\theta(\mathbf{x}_t, t, y) - \boldsymbol{\epsilon}\|_2^2])]$. The primary difference between these two is the placement of the expectation over T for LM $(1 + N)$, which is outside the function f. This arrangement implies that the randomness associated with t also aids in smoothing out local extrema, leading to better smoothed landscape and higher robustness. It is essential to clarify that this is not a result of the stochasticity hindering the evaluation of their robustness. We have already accounted for their stochasticity by applying EOT 100 times, as illustrated in Fig. 2(a). Note that the likelihood maximization acts like a pre-processing module, and it can be used to defend against adversarial attacks to any models in a plug-and-play manner, including current threat models toward large vision-language models (Wei et al., 2023b; Dong et al., 2023).

Comparison between different RDCs. As shown in Table 3, our vanilla RDC attains 73.24% ℓ_∞ robustness and 80.27% ℓ_2 robustness, surpassing prior adversarial training and diffusion-based purification techniques. By substituting the LM with the enhanced likelihood maximization, we manage to further boost the robustness by 6.83% and 4.49% against the ℓ_∞ and ℓ_2 threat models, respectively. When employing multi-head diffusion, the RDC's time complexity significantly diminishes, yet its robustness and accuracy remain intact. This underscores the remarkable efficacy and efficiency of our proposed RDC.

Table 7. Performance of DiffPure when using different architectures and checkpoints.

Method	Architecture	Diffusion model	Clean Acc	Robust Acc	
				ℓ_∞ norm	ℓ_2 norm
DiffPure	UNet+WRN-70-16	Score-SDE	90.97%	43.75%	55.47%
DiffPure	UNet+WRN-70-16	EDM	92.58%	42.27%	60.94%
RDC	UNet	EDM	89.85%	75.67%	82.03%

Ablation studies on diffusion checkpoints. We also implemented DiffPure using EDM checkpoints, decoupling the selection of checkpoints and samplers. One can use EDM checkpoints with EDM samplers or previous DDIM/DDPM samplers. The code can be found in our repository mentioned in the abstract. As shown in Table 7, when using EDM checkpoints, there is a slight improvement in clean accuracy and ℓ_2 robustness. However, DiffPure still lags significantly behind our method, as diffusion models still cannot completely purify the adversarial perturbations for the subsequent discriminative classifiers.

Attacks using multiple EOT steps. Since our methods only induce a small randomness on the gradient (see Fig. 2(a)), the Expectation Over Transformations (EOT) does not help when attacking our defense. We evaluate the robustness on the first 64 samples of the CIFAR-10 test set against the ℓ_∞ threat model with $\epsilon_\infty = 8/255$, using EOT numbers of 1, 5, and 10, respectively. Under all evaluations, RDC achieve 68.75% robustness.

B.3. Experiment on Restricted ImageNet

Datasets and training details. We conduct additional experiments on Restricted ImageNet (Tsipras et al., 2019), since Karras et al. (2022) provides off-the-shelf conditional diffusion model for imagenet dataset. Restricted ImageNet is a subset of ImageNet with 9 super-classes. For robustness evaluation, we randomly select 256 images from Restricted ImageNet test set due to the high computational cost of the attack algorithms, following Nie et al. (2022).

Hyperparameters and robustness evaluation. We use the same hyper-parameters and robustness evaluation as in Sec. 4.1. Following common settings in adversarial attacks (Wong et al., 2020; Nie et al., 2022; Zhang et al., 2024), we only evaluate ℓ_∞ robustness with $\epsilon_\infty = 4/255$ in this subsection.

Compared methods. We compared our method with four state-of-the-art adversarial training models (Engstrom et al., 2019; Wong et al., 2020; Salman et al., 2020; Debenedetti et al., 2022; Wei et al., 2023a) and DiffPure (Nie et al., 2022). For discriminative classifiers such as adversarially trained models, DiffPure, and LM, we compute the logit for each super-class by averaging the logits of its associated classes. For our RDC, we select the logit of the first class within the super-class to stand for the whole super-class.

Results. As shown in Table 9, our RDC outperforms previous methods by +1.75%, even though RDC only uses the logit of the first class of each super class for classification. This demonstrates that our method is effective on other datasets as well.

B.4. Experiment on CIFAR-100

We also test the robustness of different method against ℓ_∞ threat model with $\epsilon_\infty = 8/255$, following the same experimental settings as CIFAR-10. Due to the time limit, we only random sample 128 images. The results are shown in Table 8.

We find that RDC still achieves superior result compared with the state-of-the-art adversarially trained models and DiffPure. More surprisingly, we discover that DiffPure does not work well on CIFAR-100. We guess this is because CIFAR-100 has more fine-grained classes, and thus a small amount of noise will make the image lose its semantic information of a specific class. Hence, DiffPure is not suitable for datasets with more fine-grained classes but small resolution. This experiment indicate that our methods could be easily scaled to fine-grained datasets.

B.5. Discussions.

O.O.D. Detection. We test both the unconditional ELBO and the likelihood (expressed in Bits Per Dim (BPD) as mentioned in Papamakarios et al. (2017)). We evaluate these metrics on the CIFAR-10 test set and CIFAR10-C. As demonstrated in Fig. 3, while both methods can distinguish in-distribution data from certain types of corruptions, such as Gaussian blur and

Table 8. Clean Accuracy (%) and robust accuracy (%) on CIFAR-100.

Method	Clean Acc	Robust Acc
WRN40-2	78.13	0.00
Rebuffi et al. (2021)	63.56	34.64
Wang et al. (2023b)	75.22	42.67
DiffPure	39.06	7.81
DC	79.69	39.06
RDC	**80.47**	**53.12**

Table 9. Clean accuracy (%) and robust accuracy (%) of different methods in Restricted ImageNet.

Method	Clean Acc	Robust Acc
Engstrom et al. (2019)	87.11	53.12
Wong et al. (2020)	83.98	46.88
Salman et al. (2020)	86.72	56.64
Debenedetti et al. (2022)	80.08	38.67
DiffPure (Nie et al., 2022)	81.25	29.30
RDC (ours)	**87.50**	**58.40**

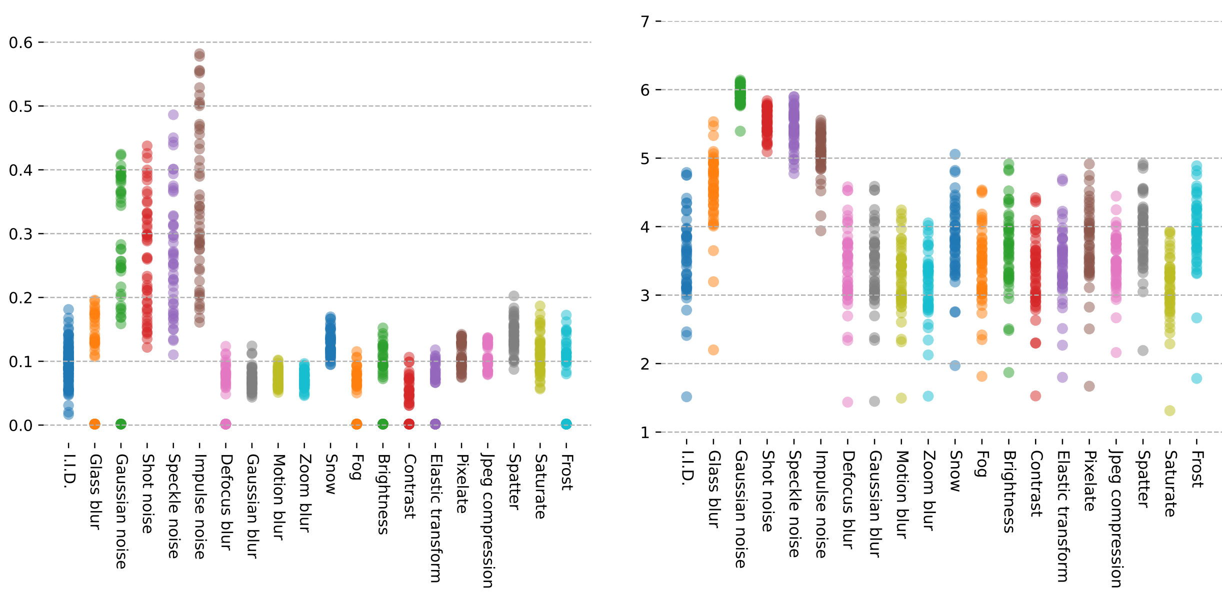

(a) ELBO on CIFAR10-C (b) BPD on CIFAR10-C

Figure 3. The prediction of ELBO and BPD on CIFAR-10 test set and CIFAR-10-C.

Gaussian noise, they struggle to differentiate in-distribution data from corruptions like fog and frost.

Generation of multi-head diffusion. Since our multi-head diffusion is initialized from an unconditional EDM and distilled by a conditional EDM, it achieves a generative ability comparable to EDM. The images generated by our multi-head diffusion are shown in Fig. 4.

C. Limitations

Despite the great improvement, our methods could still be further improved. Currently, our methods requires $N + T$ NFEs for a single images, and applying more efficient diffusion generative models (Song et al., 2023; Shao et al., 2023; Liu et al., 2023) may further reduce T. Additionally, while we directly adopt off-the-shelf diffusion models from Karras et al. (2022), designing diffusion models specifically for classification may further improve performance. We hope our work serves as an encouraging step toward designing robust classifiers using generative models.

Figure 4. The images generated by multi-head diffusion.